MASARYKOVA
UNIVERZITA

PŘÍRODOVĚDECKÁ FAKULTA

Návrh elektronového zdroje pro elektron-pozitronový urychlovač FCC-ee

Bakalářská práce

TOMÁŠ BŘEZINA

Vedoucí práce: Dr. Tomáš Radlička

Ústav fyziky kondenzovaných látek

Brno, jaro 2022

MUNI
PŘÍRODOVĚDECKÁ
FAKULTA

Bibliografický záznam

Autor:	Tomáš Březina Přírodovědecká fakulta Masarykova univerzita Ústav fyziky kondenzovaných látek

Název práce:	Návrh elektronového zdroje pro elektron-pozitronový urychlovač FCC-ee
Studijní program:	Fyzika
Obor:	Fyzika
Vedoucí práce:	Dr. Tomáš Radlička
Akademický rok:	2021/2022
Počet stran:	20 + 91
Klíčová slova:	lineární urychlovač, fyzika urychlovačů, FCC-ee, částicová optika, prostorový náboj, fotoefect

Bibliographic record

Author:	Tomáš Březina Faculty of Science Masaryk University Department of Condensed Matter Physics

Title of Thesis:	Electron source and pre-injector design for the FCC-ee
Degree Programme:	Physics
Field of Study:	Physics
Supervisor:	Dr. Tomáš Radlička
Academic Year:	2021/2022
Number of Pages:	20 + 91
Keywords:	linac, photoinjector, FCC-ee, particle accelerator, space charge, accelerator physics, particle optics, photoefect

Abstrakt

Zdroje částic pro fyziku urychlovačů jsou moderní vědní obor se zajímavou fyzikou a inženýrstvím. V této práci studujeme možnost RF-fotoinjektoru jako zdroje elektronů pro nový navrhovaný urychlovač leptonů FCC-ee v CERNu (Evropská organizace pro jaderný výzkum) a hodnotíme jeho proveditelnost.

Pomocí dvou optimalizačních algoritmů, manuálního a automatického, zjišťujeme možnosti různých možností počátečního uspořádání částic a jejich vliv na výkonnost fotoinjektoru. Výkonnost obou optimalizačních procesů je hodnocena. Kód pro sledování částic A Space Charge Tracking Algorithm (ATSRA) byl použit k simulaci chování částic v injektoru včetně efektů prostorového náboje a vnějších elektromagnetických polí.

Je diskutován materiál pro emitor elektronů a jako nejvýhodnější se jeví možnost PEA polovodiče. Byly použity dvě možnosti pro shlukovou strukturu emitovaných částic, gaussovské a rovnoměrné rozložení. Obě byly optimalizovány a bylo vyhodnoceno, že RF-fotoinjektor je vhodnou volbou jako zdroj elektronů pro FCC-ee díky jeho nízké celkové emitanci a jednoduchým použitým optimalizačním procesům.

Abstract

Sources of particles for accelerator physics is a modern scientific field with interesting physics and engineering behind it. In this thesis we study the RF-photoinjector option as an electron source for the proposed new lepton collider FCC-ee at CERN (the European Organization for Nuclear Research) and assess its feasibility.

We determine the capabilities of different options for the photoinjector, trough two optimisation algorithms, manual and automatic, we look into the possibilities of different options for the initial arrangement of particles and their effect on the performance of the photoinjector. The performance of each optimisation process is evaluated. The particle tracking code A Space Charge Tracking Algorithm (ATSRA), has been used to simulate the particle behaviour in the injector including space charge effects and external electromagnetic fields.

The material for the electron emitter is discussed and the option of PEA semiconductor seems to be the most favourable option. Two options for the bunch structure of the emitted particles were used, the Gaussian and uniform. Both of them were optimised and it was assessed that the RF-photoinjector is a valid option as a electron source for the FCC-ee, thanks to its low overall emittance and simple optimisation processes used.

MUNI
SCI

MASARYKOVA UNIVERZITA
PŘÍRODOVĚDECKÁ FAKULTA
KOTLÁŘSKÁ 2, 611 37 BRNO
IČ: 00216224
DIČ: CZ00216224

ZADÁNÍ
BAKALÁŘSKÉ PRÁCE

Akademický rok: 2021/2022

Ústav:	Ústav teoretické fyziky a astrofyziky
Student:	Tomáš Březina
Program:	Fyzika
Obor:	Fyzika

Ředitel *ústavu* PřF MU Vám ve smyslu Studijního a zkušebního řádu MU určuje bakalářskou práci s názvem:

Název práce:	Návrh elektronového zdroje pro elektron-pozitronový urychlovač FCC-ee
Název práce anglicky:	
Jazyk závěrečné práce:	angličtina

Oficiální zadání:
Student se bude zabývat návrhem a simulacemi, fotoemisního elektronového zdroje pro novou generaci elektron-pozitronového urychlovače. Součástí bakalářské práce bude fyzikální popis elektronové emise, návrh elektronového zdroje a následného lineárního urychlovače. Dále se bude práce soustředit na případné korekce návrhu pro získání optimálních fyzikálních vlastností elektronového zdroje.

Vedoucí práce:	Mgr. Tomáš Radlička, Ph.D.
Datum zadání práce:	27. 10. 2021
V Brně dne:	20. 5. 2022

Zadání bylo schváleno prostřednictvím IS MU.

Tomáš Březina, 14. 12. 2021
Mgr. Tomáš Radlička, Ph.D., 7. 1. 2022
prof. Mgr. Dominik Munzar, Dr., 14. 1. 2022

Poděkování

This thesis was created at CERN, where I was an intern for a year, under the leadership and guidance of Dr. Stefen Döbert and finished with guidance of Dr. Tomáš Radlička from ÚPT AV ČR and Masaryk University in Brno. I am grateful to both of them for their assistance and patience. I wish to thank CERN for this opportunity.

Tato práce byla vypracována během mého ročního studijně pracovního pobytu v CERNu pod vedením Dr. Stefena Döberta a dokončena byla v České republice pod vedením Dr. Tomáše Radličky z ÚPV AV ČR a Masarykovy univerzity. Jsem neskonale vděčný oběma mým vedoucím za jejich pomoc a trpělivost. Také bych chtěl poděkovat CERNu za příležitost tuto práci tam vytvořit.

Prohlášení

Prohlašuji, že jsem svoji bakalářskou práci vypracoval samostatně s využitím informačních zdrojů, které jsou v práci citovány.

Tomáš Březina

Obsah

Seznam tabulek

Seznam obrázků

1 Introduction

The European Strategy for particle physics recommended to study the implementation of a future circular lepton collider at CERN called FCC-ee (Future Circular Collider - electron positron) [1] with the aim of, amongst others, to study in detail the newly found Higg's bosson. This machine is one of the options for new high energy accelerator at CERN. It would follow up the LHC (Large Hadron Collider) as the new high energy frontier of particle physics with collision energy of the order of 100 TeV.

It is known from previous experiments, that collisions of lepton particles are much better behaved and so it enables us to study the exotic particles made from such collisions in better detail. On the other hand acceleration of leptons is much more difficult, because of their lower energy meaning they require much larger radius of the collider ring than hadrons for the same collision energy.

The injector chain consist of an electron pre-injector up to 200 MeV, an injector LINAC up to 1.5 GeV, a damping ring followed by a booster LINAC which accelerates the particles up to 6 GeV. At this energy level injection into the SPS synchrotron is envisaged followed by a booster ring and final injection into the collider ring. For positron production the 6 GeV electron are impinged on a target and captured by a 200 MeV positron pre-injector. Afterwards the positrons use the same injector chain as described for the electrons above. This thesis describes the electron pre-injector of this injector chain. There are two main options for electron sources for such a machine, an RF photo injector or a thermionic gun. The thesis comprises the source itself and a linear accelerator to accelerate the electrons up to 200 MeV. The source includes cathode as the emitter of the electrons, RF-gun and a magnetic focusing element.

The aim for this thesis is to study the potential of the RF photo injector option. In order to do so, some optimisation techniques were developed and used to get this options best performance to be compared with the thermionic gun option.

2 Theoretical background

2.1 Electron emission

Electrons are emitted from the surface of the cathode via photoelectric effect, first described by Hertz in 1887 and confirmed by subsequent observations by Hallwachs and Lenard 1888-1902 and later explained with quantum nature of light by [2]. When photons get in the cathode, they are being absorbed there by the electrons. If an electron after absorption has energy above the material work function, there is a chance, that the electron will escape the cathode. We assume that the thermal energy of electrons is much lower than the work function ($kT << \phi$) as shown in Fig. 2.1 i.e. that the cathode is at $T = 0$. The number of electrons emitted by one photon through photo emission is called quantum efficiency QE and, if the photons have enough energy, is determined by scattering phenomena effecting the electron momentum at the surface.

For description of this process, we assume the three step process described in [3]. In the first step, the photon is absorbed by the electron. In the second step, the electron travels to the surface. And in the third step, the electron is emitted through the surface, if the normal (to the surface) part of its momentum is sufficient

$$\begin{aligned} E_{max} &= \hbar\omega - \phi \\ E_0 &= \hbar\omega + E_f \ \wedge \ E_1 = E_0 - \phi \\ \mathbf{p}_0 &= \mathbf{p}_{n0} + \mathbf{p}_{t0} \ \wedge \ \mathbf{p}_1 = \mathbf{p}_{n1} + \mathbf{p}_{t0} \\ \mathbf{p}_{n1} &= \sqrt{\mathbf{p}_{n0}^2 - 2m\phi}\, \mathbf{p}_{n1}^0, \end{aligned} \tag{2.1}$$

where $\hbar\omega$ is the photon energy with angular frequency ω and ϕ is the material work function. For interested readers, details of this process are described in Appendix A. As can be seen from Eq. 2.1 the tangential momentum of the particle is preserved, and if we assume that after absorption the momentum distribution is isotropic than after emission the momentum distribution is anisotropic. The distribution of momentum creates so called intrinsic emittance explained in Sec. 2.3. and needs to be considered as the lowest achievable emittance.

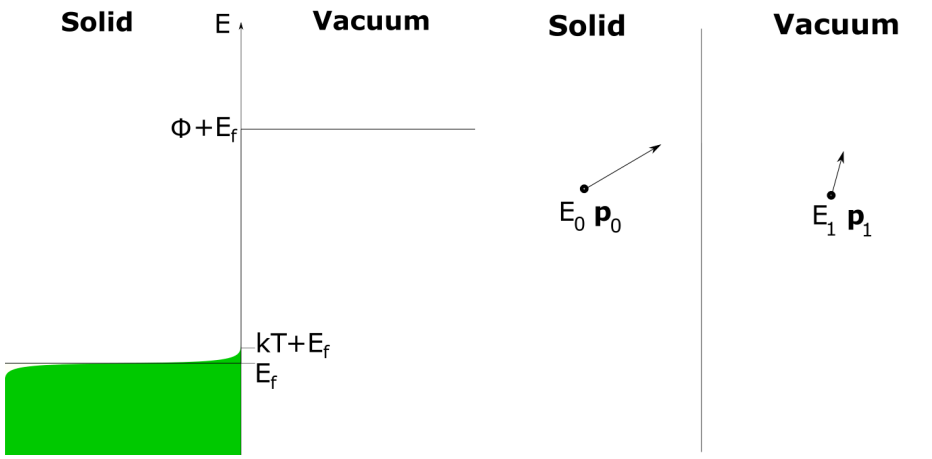

Obrázek 2.1: Diagram of distribution of electrons in solid at temperature T as a function of energy E with comparison to energy of an electron in vacuum (left).

2.2 RF cavities

The radio frequency cavity is a piece of equipment used as the accelerator in the high energy accelerator physics. There are two main types of such cavities, a standing wave structure, used primarily in circular colliders and accelerators, such as synchrotrons and cyclotrons, and RF electron guns and a travelling wave structure used almost exclusively in linacs.

2.2.1 Standing wave cavity

The main idea for the standing wave cavity is that the frequency of the rf wave in the cavity is synchronised with the speed of the beam travelling through the cavity, so the beam is only affected by a positive electric field in order to be accelerated. For interested reader full derivation of the fields in SWSs (standing wave structure) are given in Appendix B, here we shall only present final results. From all of the existing modes we are only interested in two modes; the fundamental mode TM_{100} and TM_{101}. We omit presenting the magnetic parts of the modes since they are affecting the beam only marginally. The fundamental mode is the only mode, that has non-vanishing effect on

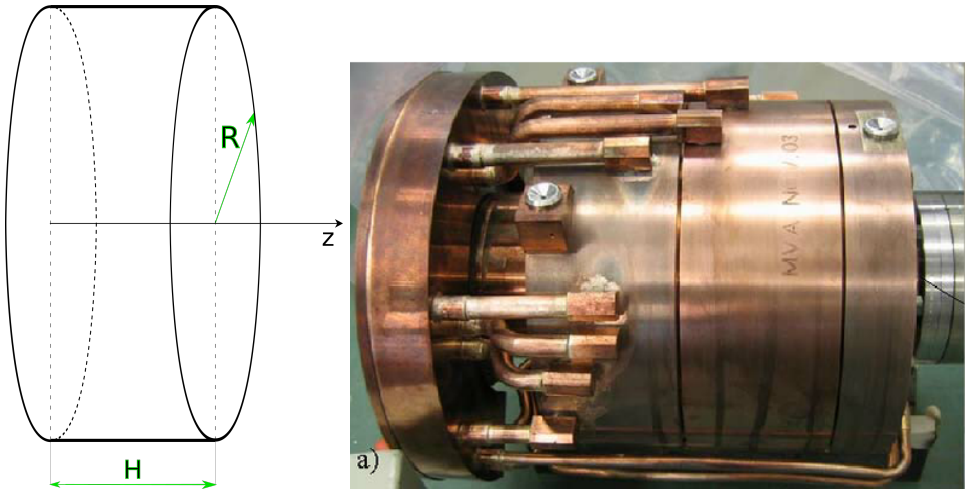

Obrázek 2.2: Pillbox cavity (left). DESY L band 15 cell RF Gun cavity (right) [4].

acceleration and have only the longitudinal electric field non-zero

$$E_z = E_0 J_0(p_{10} r) e^{-i\omega t}. \tag{2.2}$$

On the other hand the TM_{101} mode is responsible for the focusing effects of the cavity, because of its non zero radial electrical component and is explicitly derived in Eq. 2.3.

$$\begin{aligned} E_r &= -E_0 \frac{\pi R}{p_{10} H} J_1\left(\frac{R}{p_{10}} r\right) \sin\left(\frac{\pi}{H} z\right) e^{-i\omega t} \\ E_\theta &= 0 \\ E_z &= E_0 J_0\left(\frac{R}{p_{10}} r\right) \cos\left(\frac{\pi}{H} z\right) e^{-i\omega t} \end{aligned} \tag{2.3}$$

As is obvious, we always make the optical axis same as the axis of the wave guide (z axis) as to have cylindricaly symmetrical solution and maximum acceleration.

The SWSs are made from multiple cell of perturbed pillboxes, not only a single one. The special case of SWS is RF-gun, since its first cell is cut in half, as to achieve maximum gradient at the position of

electron emission. The SWS in this work is used as the RF-gun at the begging of the beam line described later in Ch. 3.

2.2.2 Travelling wave cavities

For this section works of [5] and [6] are being used extensively. The travelling wave structures are used to energize already highly relativistic ($\beta \simeq 1$) particles, mostly electrons, so that the phase velocity of the cavities can be constant ($v_{ph} = c$) and still energize the electrons. Further reading is provided in cited sources and Appendix B, here we shall only present results without derivations.
There are two principles that theoretically lead to electron gaining

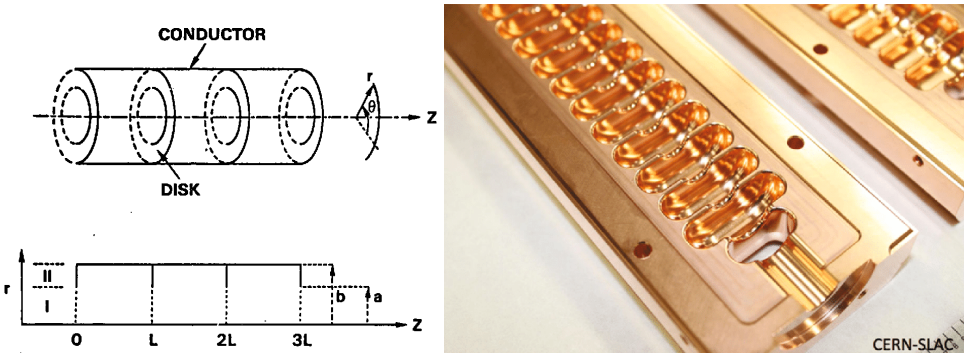

Obrázek 2.3: Disk loaded waveguide (left). The split X-band accelerating structure for the CLIC collider (right) [7].

energy when travelling in straight line. First one is using waveguide for which the electromagnetic field is computed similar to the standalone cavity, but there is no boundary condition in z direction. This solution gives the EM wave phase velocity greater than c which means it is unusable for acceleration. The second approach would be to arrange a series of individually powered pillbox cavities. This, in theory, would work perfectly, but from the practical point of view, to arrange these many cavities (we are talking about hundreds at a time) is too complex and to have individual power source for each and every one of them would be incomprehensibly expensive. This leads us to a compromise between these two approaches, the periodically loaded structure. The

periodically loaded structure is the only TWS used in this work for the reasons mentioned above.

The solution for the electric field in the transverse plane is the same as is for the pillbox cavity, and in the longitudinal direction we aim to have propagating wave with phase velocity $v_p = c$ and wavelength $\lambda = md$ where d is spacing of the disks and m is integer labeling the long. mode of the structure (for example $2\pi/3$ mode is where the wave spans across 3 cells).

It is important to say, that the periodically loaded waveguides have major limitation of RF breakdown, which limits their performance as high gradient structures. In order to maximise the voltage gradient of the TWS we need to use very smooth surfaces and cryogenically cooled superconducting materials such niobium and its alloys and compounds. Since the geometrical description of such superconducting RF cavities is not trivial the description of the electromagnetic fields is not even possible analytically speaking, so only numerical models are used in this case using codes such as Poisson Superfish. In this work we will be using measured values of existing structures in use, mostly used in the SwissFEL facility at the PSI.

2.3 Transport dynamics

In order to quantify the beam qualities, we need to use more than simply tracing behaviour of every particle in the beam under the influence of the magnetic and electric fields. Since we are dealing with ensemble of particles, it is convenient to describe it as such. Generally, the phase space and Hamilton equations are used to describe particle dynamics but for the most of our purposes, we do not need such general approach so in this section we will describe and derive the necessary theory and simplifications of the beam dynamics.

2.3.1 Phase space

Let's consider a particle moving in typical Cartesian 3D coordinate system x, y, z with some momentum p_x, p_y, p_z. This particle can be completely represented by a set of six variables x, y, z, p_x, p_y, p_z with t time as a parameter. Those parametres create six dimensional space

known as phase space. Description of dynamic system in six dimensions is not possible in visual terms, so in order to visualise the information, we visualise three two-dimensional parts of the phase spaces for each coordinate and its respective momentum. In addition we look at the beam in real 3D space.

For the sake of convenience we transform our set of variables so that z is the parameter since the beam travels along the optical axis with small deviations, so we get x, y, t, x', y', E where we can distinguish transverse variables x, y, x', y' and longitudinal variables t, E

$$\begin{aligned} p_\alpha &= \gamma m \frac{d\alpha}{dt} = \gamma m \frac{d\alpha}{dz}\frac{dz}{dt} = \gamma m \beta c \alpha'; \alpha = x, y \\ p_z &= \gamma m \beta = E\frac{\beta}{c^2} \\ \alpha(t) &= \alpha(t(z)) \Longleftrightarrow \alpha \equiv \alpha(z); \alpha = x, y \\ z &= f(t) \Longleftrightarrow t = f^{-1}(z), \end{aligned} \tag{2.4}$$

where we assume that $p \simeq p_z$ and that $f(t)$ has an inversion function.

The Eq 2.4 correctly works only when the average energy of the beam remains constant, however we still use this variable for its usefulness describing the beam and later in this chapter is explained, how we deal with the new phase space under acceleration. In order to work in phase space, we use Liouville's theorem, which is derived from the Hamiltonian approach, as described in [8]. Here are presented only the results and limitations of the theorem.

The theorem states that the particle density in any hyper volume of the phase space remains constant along the particle trajectory. In other words, the particle distribution in the beam can change in phase space, the overall volume cannot. This is under the assumption that the only forces acting upon the beam can be derived from Hamiltonian, which doesn't include any dissipation forces like synchrotron radiation, or interaction within the beam like space charge. Now the most important implication of this theorem can be seen, if the three components of motion are mutually independent, this means, that area occupied by the beam in phase space corresponding to any coordinate remains the same throughout the movement.

2.3.2 Emittance

The area occupied by a beam in a modified phase space is known as emittance $[\varepsilon_x] = \pi\, mm\, mrad$ (since the most general shape of a beam in phase space is ellipse which has area of $S = \pi ab$, it only makes sense to present the numerical result divided by π). When we take uncoupled movement of particle moving in a restoring force field (such as FODO lattice for transversal coordinates or RF cavity for longitudinal coordinate) the movement is the same as the movement of a harmonic oscillator, which in phase space means, that the particle movement has a eliptical trajectory in phase space shown in Fig. 2.4.

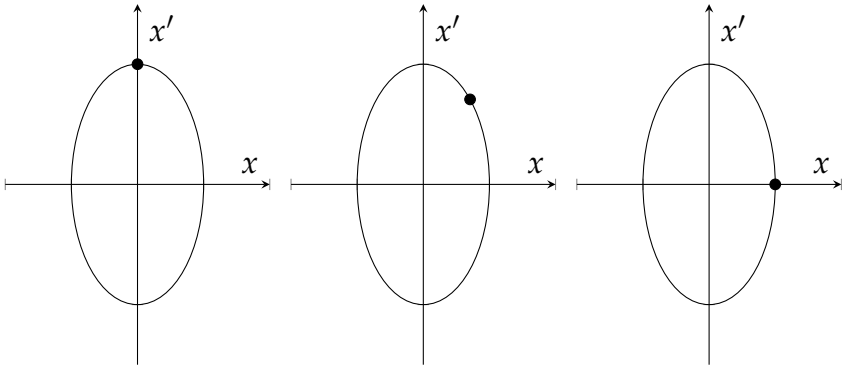

Obrázek 2.4: The phase space trajectory of single particle under harmonic force

A real beam has no hard edge boundary. In order to determine the emittance of the beam, we encompass certain percentage of the beam charge with an ellipse in a phase space and the area of the ellipse determines the emittance (the ellipse with the least emittance is always chosen) called geometric emittance. Or equivalently, we can determine the rms value of the emittance, which is widely used, because of its simple determination

$$\varepsilon_{x,rms} = \sqrt{\langle x^2 \rangle \langle x'^2 \rangle - \langle x x' \rangle^2}. \tag{2.5}$$

Here we should say, that the above equation calculates the emittance of the whole ensemble, since we can calculate the emittance of a single

particle, but this won't be of a concern in this thesis. Now should be said why do we even bother calculating emittance.

If we take the phase space diagram and let the beam transport through some system, we can draw a boundary in the phase space diagram at any point of the transport system. If a particle is outside this boundary, it is lost in transport. We call this boundary admittance. If the emittance is larger than admittance, there will always be some beam loss, however even if the emittance is lower there can still be a loss if the shape of the beam in a phase space is different than the shape of the admittance. For an interested reader more can be found in [9].

The other reason, why we want to have as low emittance as possible is apparent when we take a look at parameter called luminosity, which corresponds to a rate of events of two colliding beams $\mathrm{d}R/\mathrm{d}t = L\,\sigma_p$ where σ_p is interaction cross section,

$$\begin{aligned} L &= \frac{f N_b N_1 N_2}{2\pi\sigma^2} \\ L &= \frac{f N_b N_1 N_2}{4\varepsilon\beta^*} \end{aligned} \tag{2.6}$$

where we used relation $\beta = \pi\sigma^2/\varepsilon$ where σ is a beam spot size and β is amplitude function (not to be confused with relative velocity $\beta = v/c$) and β^* is the amplitude function at interaction point and ε is emittance as described in [10]. The higher the luminosity at the interaction point is, the better the performance of the collider is, and since there are no good means of reducing emittance other than synchrotron radiation, we take emittance as constant of motion so we want as low emittance growth in the low energy region of the accelerator as possible. The parameter β can be adjusted by magnetooptical systems such as quadrupoles, sextupoles and higher order multipoles and won't be much of a concern in this work. Further reading about the importance of β parameter when discussing beam dynamics in circular collider can be found in [9, 11].

As mentioned above, the Liouville's theorem holds true only if all forces present are independent of a beam, that is experiencing them. This is clearly not true for space charge and the effect of the space charge on emittance will be discussed in Appendix D.

2.4 Longitudinal beam dynamics in accelerating cavity

We need to make distinction between two cavity types for which there will be two very different particle behaviours, standing wave cavity (SWS) and travelling wave cavity (TWS), whose differences are described in Section 2.2.

2.4.1 TWS

Let's first consider a case of travelling wave cavity. When a particle with energy γ_0 enters a cavity with a maximum electric intensity $\mathscr{E}_0 \equiv eE_0/mc^2$, a wave number $k = 2\pi/\lambda$, phase velocity β_p and initial phase Δ_0 of the fundamental mode of operation. Then we can create the equations of motion for the relativistic particle ($p \simeq \gamma cm$, $\beta \simeq 1$)

$$\begin{aligned} \frac{\mathrm{d}\gamma}{\mathrm{d}z} &= -\mathscr{E}_0 \sin\Delta \\ \frac{\mathrm{d}\Delta}{\mathrm{d}z} &= k\left(\frac{1}{\beta_p} - \frac{1}{\beta}\right) \end{aligned} \tag{2.7}$$

Here we neglect the higher order modes in the cavity since over long period, due to them having different phase velocity from fundamental mode, their effects are zero. By solving these equations adding the afford mention initial conditions of initial energy γ_0 and initial phase $\Delta_0 = 0$, we derive equation for trajectories in phase space, which are presented in Fig. 2.5, as derived in [8]

$$\frac{\mathscr{E}_0}{k}\cos\Delta = \frac{\gamma}{\beta_p} - \sqrt{\gamma^2 - 1} + \frac{\mathscr{E}_0}{k} - \frac{\gamma_0}{\beta_p} + \sqrt{\gamma_0^2 - 1}. \tag{2.8}$$

Here we need to distinguish two different cases, when $\beta_p < 1$ and $\beta_p = 1$. When the phase velocity is below the speed of light, the particles near the zero phase and $\beta \simeq \beta_p$ oscillate around this point similarly to pendulum, with difference being the relativistic effects. This however means that TWS with phase velocity below speed of light can be used only for very low total acceleration. When the velocity is equal to the speed of light, for particles with zero initial phase and with energy above some critical value, depending on the gradient,

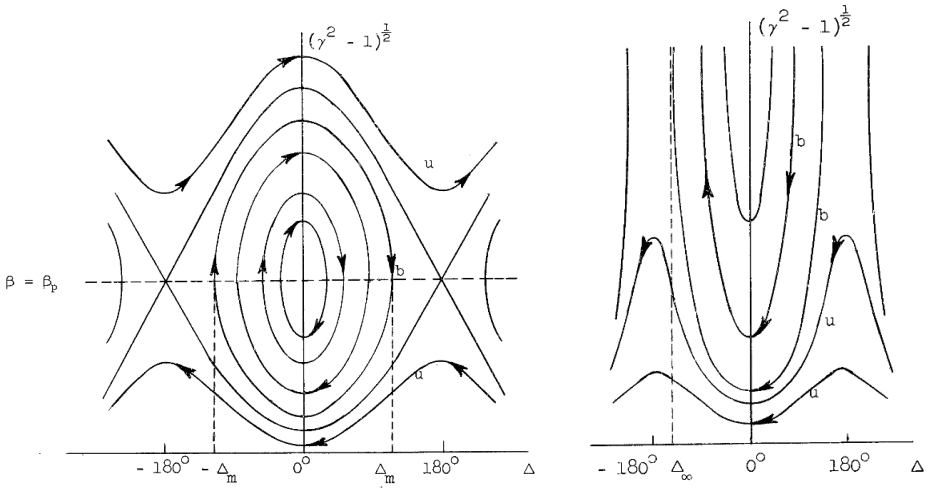

Obrázek 2.5: Phase space for $\beta_p < 1$ (left) and for $\beta_p = 1$ (right).

will be reaching some asymptotic phase Δ_∞ as derived in [8]. If the initial energy of the particle is below the critical value for both cases the overall energy gain would be zero, because the particle would always gain (lose) phase.

2.4.2 SWS

For the case of standing wave cavity, there are two possibilities, single or multiple cell. Multiple cell works very similarly to TWS. For the acceleration to be effective, we need to match the time it takes the particle to cross one cell with the period of the cavity. Here the "phase velocity", which we can define as $\beta_p = \lambda/cT$ where T is the period, is always equal to one and the actual acceleration isn't asymptotic as in TWS but periodically changes as it travels trough the cavity.

For a single cell cavity, for acceleration, it isn't required to have matched the phase velocity. Consider particle with velocity β travelling through cavity with wave length λ and maximum electric gradient E where the initial phase is Δ_0. The time it takes the particle to travel through the cavity is $t = \lambda/2c$ where we neglect the effect of the cavity on the velocity. Since the time isn't zero, initial and final phase are

different by $\delta\phi = 2\pi t/T$, which changes the energy gain depending on the initial phase and initial velocity.

2.5 Phase stability and bunch compression

Since the bunch has non zero length, each particle of it arrives in the cavity (mostly TWSs) in different times meaning they are effected by different electric field since they are in different phases of the field. In order for the beam to be stable, it is necessary that the first particle arriving in the cavity, meaning it has the largest speed and energy, is accelerated less then the last particle so that the energy gain for the difference in energy of the last and first particle is smaller than it was before entering the cavity. However this effect is negligible in linear accelerators once the particles are ultra-relativistic ($\beta \approx c$), since even a large difference in energy means little difference in velocity, so it can be assumed that the phase space is "frozen"in the longitudinal direction at high energies and does not evolve much any further. This means that the beam needs to be actively stabilised in regions of low energy. In circular accelerators this is not the case since the higher the energy the longer the orbit, so the beam evolves in phase space even in high energies.

Let's consider RF cavity with electric field $E = E_0 \cos\theta$ and bunch of particles with length l arriving in the RF cavity meaning the length in phase of the electrical field $\Delta\theta = l\lambda/c < \pi$. Position of the bunch center needs to be in $\theta = \langle -\pi/2, \pi/2 \rangle$ in order for the bunch to be accelerated. If we split this interval in half, we get two different phenomena for the bunch edges. For $\theta = \langle -\pi/2, 0 \rangle$, right edge is accelerated faster than the left edge, so the bunch stretches and bunch length increases. For $\theta = \langle 0, \pi/2 \rangle$, left edge is accelerated faster than the right edge, so the bunch compresses and bunch length decreases. We only considered the edges of the bunch where upon arrival all of the particles have the same speed, although this is simplification, it gives good idea about the effect of the wave curvature on the bunch length.

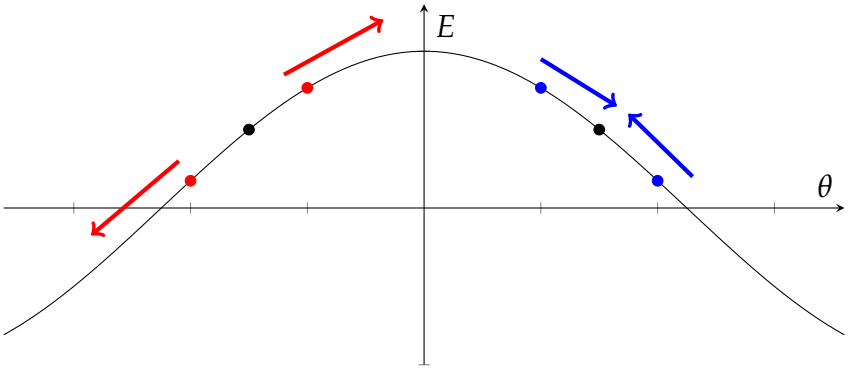

Obrázek 2.6: Diagram showing bunch stability in RF cavity where E denotes the electric field and θ denotes phase of the wave. Edges of bunches are represented by red and blue dots for unstable and stable bunch respectively. The black dots represent centers of the bunches. For simplicity the bunches are made of positively charged particles.

2.6 Space charge

Every charged particle interacts with other charged particles through Coulomb interaction. Particle beams aren't any different, however, in this context, we use a term space charge to call these interactions, since Coulomb interactions are between each two particles, here we need to describe the effect of the whole ensemble on itself, and we also include Lorentz forces created by movement of this ensemble in this term. The term space charge used here is different than is used in particle optics and is explained in next paragraph.

Let's assume we know positions of all particles in our beam. Since our beam is axisymetrical, we take a ring with the r and z position of each particle and give it the particles charge. We then proceed to calculate the fields at the beam axis each of the ring creates and then add them up. This creates new electric field on the axis with which we work in paraxial approximation.

For the FCC-ee, high current, high charge beam is planned to be used, where the space charge forces play a significant role. The intuitive analytical calculations of space charge are given in Appendix D.

2.7 Magnetic focusing

There are several ways to focus an electron beam. For low energy, non-relativistic beam electrostatic lenses are used since they are able to provide the focusing needed less expensively and less complexly then magnetic elements. When the beam gets to relativistic speeds, the focusing effect of electric fields in general is diminishing and the focusing effect of magnetic fields is rising. As mentioned in chapters above, the driving force for beam dynamics is the Lorentz force $\mathbf{F} = q\mathbf{E} + q\mathbf{v} \times \mathbf{B}$. For a quick comparison, let's assume, that we have a relativistic electron $\beta \simeq 0.8$ and a dipole magnet with strength of $B = 1$ T, which is not unusual in particle accelerators, and that the beam velocity and the magnetic field are perpendicular, the magnetic part of the Lorentz force is equal to $F_B/q = \beta cB = 240\ \mathrm{MVm}^{-1}$. The state of the art rf accelerators have gradients $E = 120\ \mathrm{MVm}^{-1}$ [12] which is still only half way through and wouldn't even be good for focusing. For medium and low energy electrons ($\beta < 1$ and $\gamma > 1$) in linacs solenoids are generally used.

An intuitive reasoning behind solenoid focusing is given in [13], [14], [15] and in Appendix C here we present only some results. Under the assumption of paraxial approximation, meaning we assume that the velocity is mostly in z direction $v_r << v_z$ and that the field is slowly varying along z (the third and higher derivatives are negligible), we derive equations for magnetic field based on their axis values $B_z(r = 0, z)$ to be

$$\begin{aligned} B_r(r,z) &= -\frac{r}{2}\frac{\partial B_z(0,z)}{\partial z} \\ B_z(r,z) &= B_z(0,z) - \frac{r^2}{4}\frac{\partial^2 B_z(0,z)}{\partial z^2}. \end{aligned} \tag{2.9}$$

These are called paraxial equation for axisymetrical magnetic field (not the equations for paraxial trajectories). From the equations of motion (which are in the rotating frame of reference)

$$\begin{aligned} \gamma m\frac{\mathrm{d}v_r}{\mathrm{d}t} &= -qv_\theta B_z + \gamma m\frac{v_\theta^2}{r} \\ \gamma m\frac{\mathrm{d}v_\theta}{\mathrm{d}t} &= -qv_\theta B_r - \gamma m\frac{v_\theta v_r}{r} \end{aligned} \tag{2.10}$$

from which we derive, under the paraxial approximation of the field, the azimutal velocity to be

$$v_\theta = \frac{qrB_z}{2\gamma m} \tag{2.11}$$

and the focal length to be

$$\frac{4}{f} = \int_{-\infty}^{\infty} \left[\frac{qB_z(0,z)}{\gamma m \beta c}\right]^2 \mathrm{d}z. \tag{2.12}$$

From Eq. 2.12 we can see that the focusing $(1/f)$ depends on the square of the magnetic field and one over square of γm which means that particles with higher energies and higher masses are focused less. In practical terms the solenoid is useful for focusing only light particles (electrons, positrons) with low energy. It is necessary that the field of the solenoid is zero at the cathode, otherwise it would introduce more emittance. We can also estimate the strength of the solenoid based on the momentum of the bunch and length of the solenoid as

$$B_0 = \pi \frac{\beta\gamma mc}{le}. \tag{2.13}$$

2.8 Simulation code - ASTRA

ASTRA includes two computational codes and three graphical programs. The first code named generator is used to generate initial distribution of makroparticles. We can set the space distribution for each axis independently, or create 2D and 3D distributions. For z axis, which is the direction of the acceleration, we usually don't set distribution in space but in time, simulating the emission process. Momentum distributions are set up the same and on this initial momentum then depends the intrinsic emittance of the beam. Here we also set the number of makroparticles and total charge of the bunch.

Since most of the time, we use bunch charges in orders of magnitude 10^{19} of elementary charge, we wouldn't be able to simulate so many particles at once. So instead we use makroparticles, which behave like clusters of the particles, with exactly the same properties.

The second code is the actual tracking algorithm (ASTRA) that takes the initial distribution from generator and user defined external

EM fields and then uses non-adaptive Runge-Kutta integration of 4^{th}order to track the particles along the trajectory. The space charge is calculated right after the emisssion (with the initial distribution of particels) as described in Sec. 2.6, where the space around the axis is divided into rings with positions (r, z) and cross sections $S = \delta z \delta r$. If in such a ring, there are makroparticles, the field at the axis is calculated as if the charge was distributed uniformly along the ring. In order to save computational time there is a formula, that analytically predicts the space charge fields, so it only fully numerically recalculates these fields after the maximum of such field changes more the user predefined factor of the initial field.
The external fields are given only on the axis and the rest of the space is calculated based on Maxwell equations in paraxial region as presented in Sec. 2.7. In this work we use only three kinds of external field maps (the distribution of the field along the axis), solenoid, SWS and TWS. For these external fields, we can set a number of parametres like the maximum field, phase offset, position on z axis, transverse offset, number of cells and others.

The outputs of astra are of two kinds. First is the text file (called "full") containing position and momentum of each makroparticle in user defined distance of the bunch from the cathode. These are the raw data we can later use for thorough analysis. The second one is part of the log text file and is read by one of the graphical program, lineplot. These data cannot be directly extracted from the file, but can be extracted from the lineplot program as data. These data contain the calculated values of emittance, bunch length, beam spot size, energy spread, average energy etc. From these, we can better see how these parametres evolved along the beam line.

The other two graphical programs are called postpro and fieldmap. Postpro reads the "full"file and displays the distributions of the makroparticles in different planes of phase space. There are also other functions, but they won't be used in this work. Fieldmap displays external fields, each type (solenoid, cavity) separately.

3 Design parametres of the photoinjector

3.1 Outline

As mentioned in the introduction, this thesis will mostly focus on the electron source, but nonetheless we should give here a brief mention about the design of the whole injector. The injector starts with an RF-photogun, followed by accelerating structures (travelling wave cavities) up to energy $E = 200\text{MeV}$, where the beam gets extracted and is worked with in following structures.

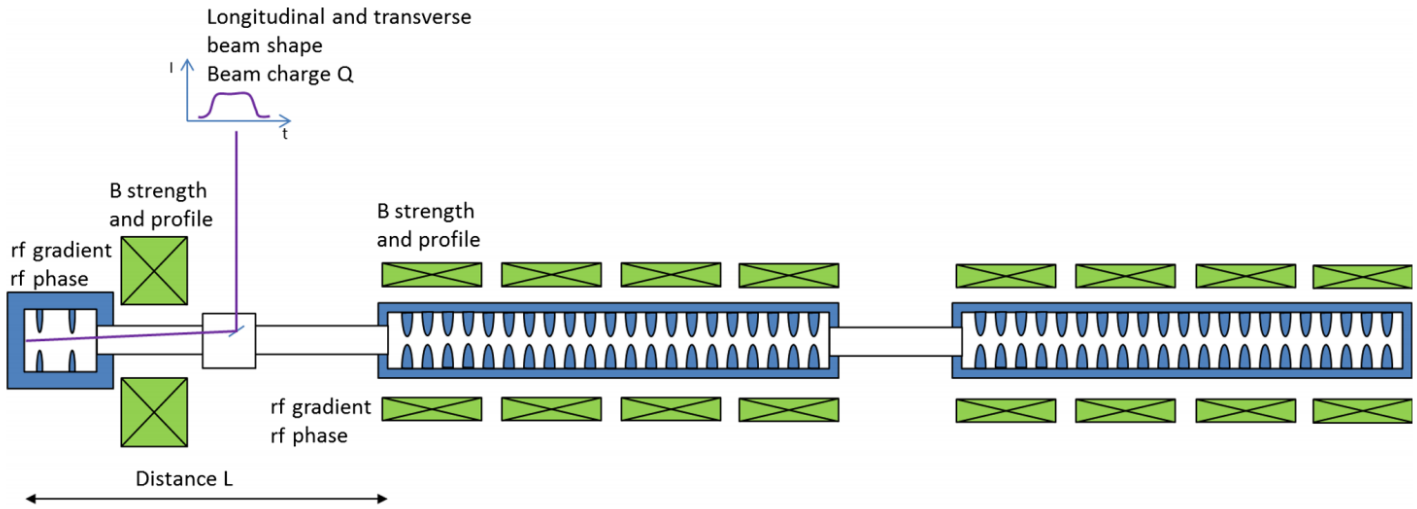

Obrázek 3.1: Basic photoinjector layout with one solenoid configuration and with the most crucial optimisation parametres mentioned.

For the time being as a realistic example of accelerating structure for simulations, we are using measured values of the TWS-PSI-Sband used in the SwissFEL at the Paul Scherrer Institut desribed in [16] and [17]. The basic parametres are given in Tab. 3.1.

The source itself is comprised of RF-gun and focusing solenoids, one around the RF-gun and one behind it. The RF-gun is also taken

Tabulka 3.1: Main paramatres of the SwissFEL S-bandr TWS

Parameter	Value
Operating frequency	2998.8 MHz
Phase advance per cell	$2\pi/3$
Total number of cells	120+2
Accelerating gradient	20 MV/m
Maximum pulse repetition frequency	100 Hz
Operating temperature	40°C

from SwissFEL at PSI for consistency and is described in [12], in Tab. 4.1 are given only the main parametres.

Tabulka 3.2: Main paramatres of the SwissFEL RF-gun

Parameter	Value
Operating frequency	2998.8 MHz
Total number of cells	2.5
Accelerating gradient	100 MV/m
mode separation	$\geq$ 15 MHz
Operating temperature	40°C

In Figs. 3.3 and 3.4 we present the fields on the axes of used structures. Since we use paraxial approximation, these are the only information needed to compute the field at any point as discussed in Sec. 2.7.

The gradient of both of these structures can be adjusted to optimise the beam parametres, for the TWS, we can do up to 30MV/m, for the RF-gun up to 120MV/m. The length of both of these structures can be derived from above mentioned parametres since we know phase advance per cell ϕ, number of cells N and frequency f, lengths are

$$l = \frac{\phi}{2\pi}\frac{c}{f}N \tag{3.1}$$

12.5 cm for the RF-gun and 4 m for the TWS. For focusing, there is a double solenoid configuration over the RF-gun and single solenoids around the TWS. As stated in Secs. 2.7, C and in [14] it is crucial to have zero magnetic field at the emitter in order to minimize emittance. To do

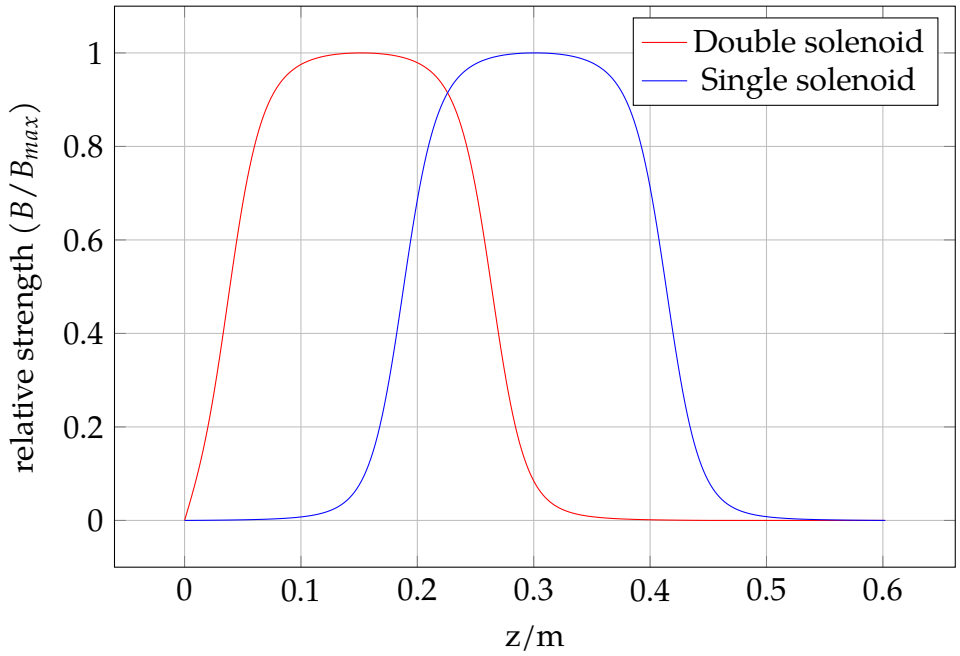

Obrázek 3.2: Comparison of double and single solenoid configurations

that we either need to place the solenoid far enough from the emitter or use two solenoids with opposite fields symmetrically around the emitter. The inherent advantage of the the double solenoid option is the much faster rise of the magnetic field (the position of the maximum is closer to the emitter) meaning faster focusing and thus reducing emittance growth from the space charge in the low energy region as explained in Sec. 2.7.

In Chapter 4 we will discuss the effect each of these configurations have on the beam and decide to use the one that performs better regarding the beam parametres, mainly emittance and beam spot size.

3.2 Required beam parametres

Here we list current requirements for the beam parametres at the end of the injector. Since the project is at the beginning, we don't have any strict boundaries, but more like guidelines for our electron source,

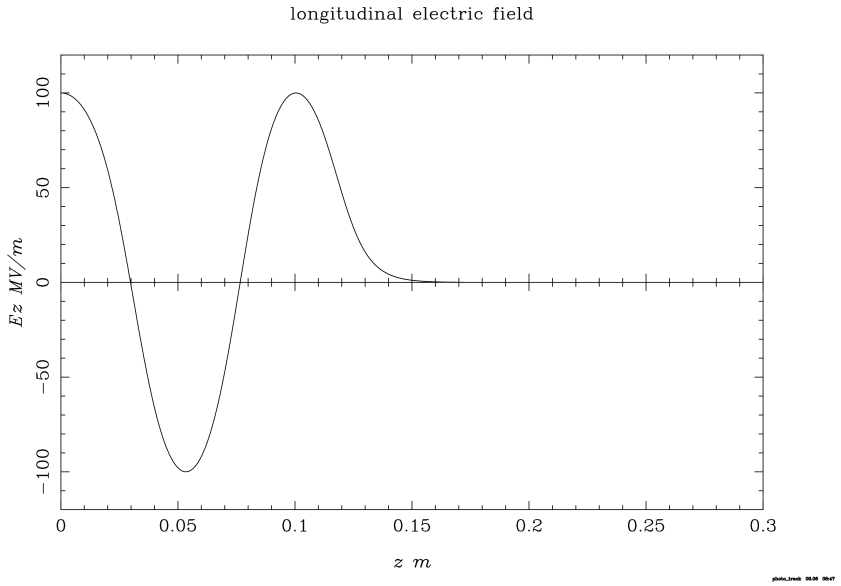

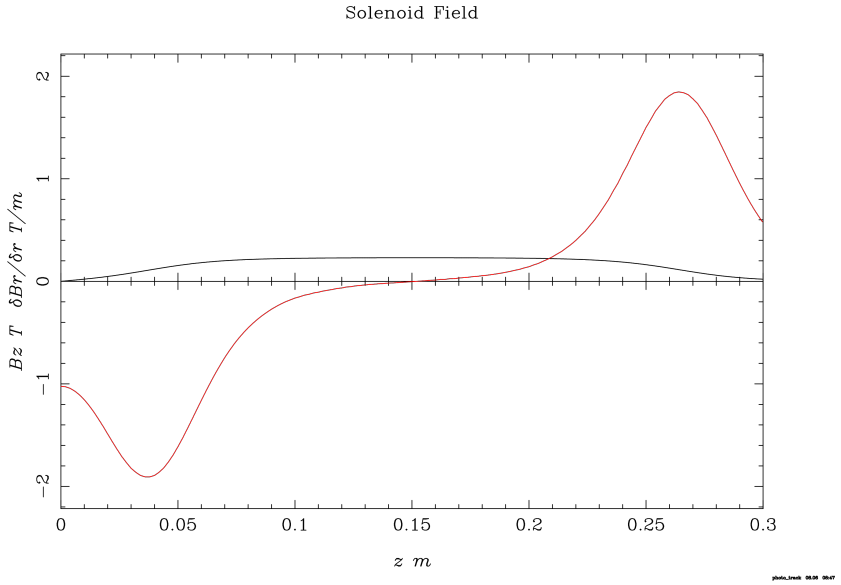

Obrázek 3.3: The amplitude of the electric field $E_z(r = 0, z)$ of the RF-gun (top). The longitudinal magnetic field $(B_z(r = 0, z)$ (black) and transversal magnetic field $\delta B_r(r, z)/\delta r$ of the solenoid used for the RF gun (bottom).

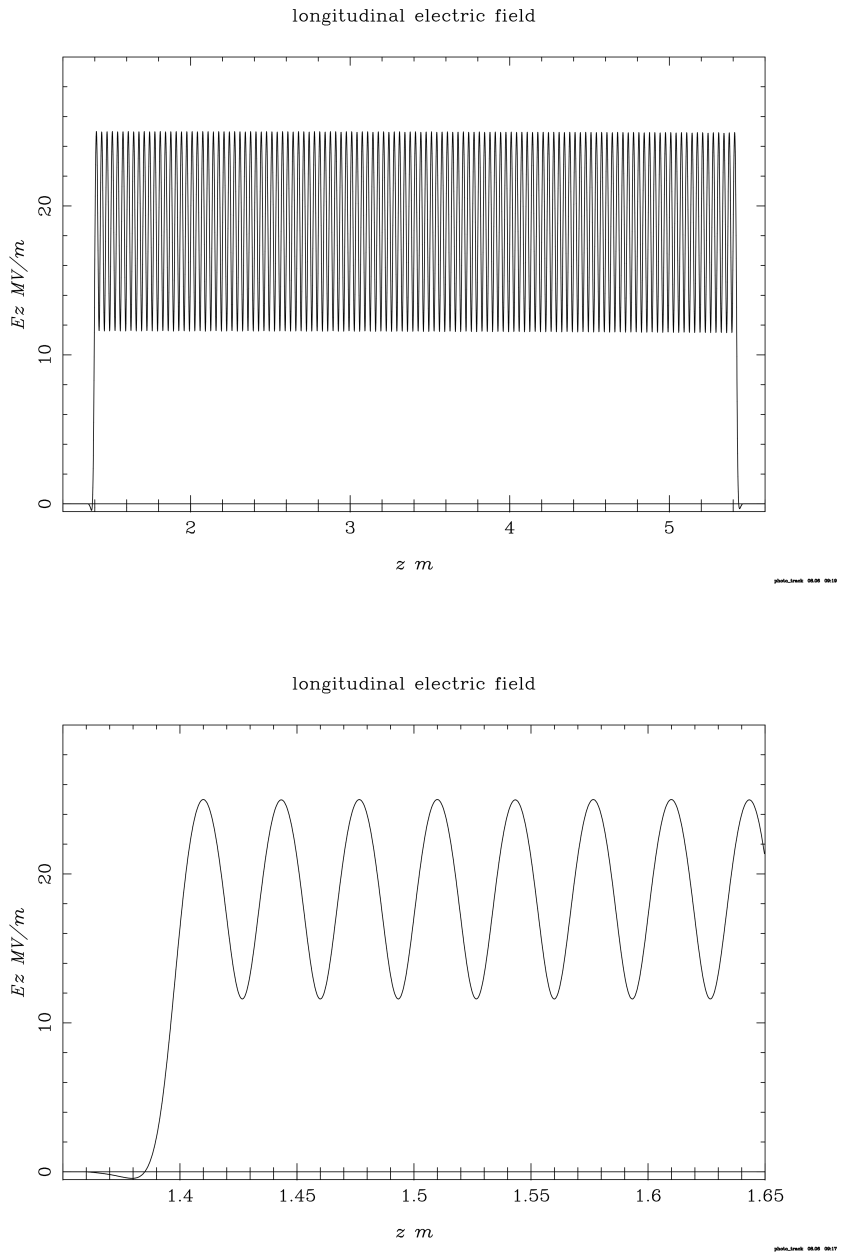

Obrázek 3.4: The amplitude of the electric field $E_z(r = 0, z)$ whole TWS (top) and in detail (bottom).

which are assumed based on previous projects and the purpose of this collider. The requirements are summed up in Tab. 3.3.

Tabulka 3.3: The known requirements for the beam at the and of the beam line of the injector.

Parameter	Requirement
Energy	200 MeV
Charge	5.0 nC
Beam size	<1.5 cm
Bunch length ($v \simeq c$)	<2 cm

3.2.1 Energy

Since the electron is very light $E_0 = 0.511\,\mathrm{MeV}$, it reaches ultra relativistic energies swiftly and as discussed above, when the relativistic effects are strong enough, the phase space effectively freezes and doesn't change, which is very important for beam extraction, because the beam doesn't gain much, or any emittance. The energy chosen to be sufficient for this purpose is $E = 200\,\mathrm{MeV}$ or $\gamma = 390$, even though the value chosen is highly artificial, for the group, working on the other systems down the beam line, it is essential, that the number is known and isn't subject to change so their works can be performed simultaneously to ours.

3.2.2 Beam size

The common apertures of S-band cavities are around 15 mm in diameter. This is the main limitation of transversal beam size. Though it is possible to enlarge the aperture of the cavity it would make it less energy efficient and so we want to avoid it if possible. There is also a limitation on minimal beam size at the cathode due to the space charge forces increasing with decreasing volume of the bunch but at the end the space charge forces are negligible so there isn't any limitation on the minimal beam size.

3.2.3 Emittance

There are several configuration of the electron-positron injector in consideration and emittance at the end of the electron injector is the main driving decision factor. So the emittance doesn't have any hard limits but certain schemes and configurations of systems down the line have. Also it needs to be decided between optimisation of the energy spread (essentially a longitudinal emittance) or the transversal emittance since when optimised, lowering one means increasing the other, see Liouville's theorem in Sec. 2.3.

3.2.4 Charge

In [1] it is decided that the operating charge of a bunch of the FCC-ee will be $Q = 3.2$nC for both particle species. Since the current scheme involves positron production by bombarding a target with electrons from our source to save cost by using the same structures, we need to have a margin for the positron production. The initial proposals were counting with 50% conversion rate, which we now know is an underestimation, and is much closer to 100%. Even for the unity conversion rate we aim to have 50% margin this early in development. This means that the electron bunch charge for the positron production is to be $Q = 5$nC.

3.2.5 Bunch length

Since the bunch length doesn't change much in the accelerator, it is solely dictated by the emission time. The bunch length has no major restrictions itself, though we need to count with the RF curvature and so the bunch length has direct effect on the energy spread. The effect the emission time has on the RF curvature induced energy spread is shown in Fig. D.3. These are the upper limits of the bunch length but because of the space charge, we need to count with large enough margin to achieve those energy spread values in reality.

3.2.6 Phase space contours

The admittance as mentioned does not restrict only the overall emittance of the beam but also the shape the beam has in the phase space.

For our purposes it was decided that longitudinal distribution at the end of the beam line is to be constant in space (or as close as possible to it) and have peak with short tail in momentum (the shorter and lower populated the tail is, the better). The transversal distribution is to be radially Gaussian in both space and momentum. The lower the deviations of these distributions are, the better the configuration is optimised.

4 Beam simulation and optimization

There are many parametres that could be optimised regarding both the beam emission and structures. Trying to optimise them all at once would be to time consuming and would result in only slightly better quality of the beam, so we have chosen the parametres for which we can't reasonably analytically predict their effect on the beam and that have the most significant effect with the least amount of change.

These parametres were sorted into three categories: first are the most significant ones that need to be optimised all at once being the initial spot size, first TWS gradient, first TWS position and solenoid strength; in the second category are parametres whose effect on the beam we can predict at least semi-analytically, initial spot size (this is included in both categories and is explained why later in this chapter), emission time, gun gradient and phase offset; and in the third category are parametres that don't effect the beam parametres much and can be optimised one by one after the previous categories were optimised. Since this work is done before actual outline and elements were chosen, optimising the third category, which would result in only minor change in the beam parametres, wouldn't make sense, because the difference made due to different outline would be more significant.

Tabulka 4.1: Parametres most suitable for optimisation

Parameter
Initial beam size
Emission time (initial bunch length)
Accelerating gradient of RF-gun
Phase offset of the RF-gun
RF-gun solenoid magnetic field strength
Accelerating gradient of each TWS
Phase offset of each TWS
TWS solenoids magnetic field strength
Position of TWS

First of all we need to address the issue of generating two different bunch charges for two different purposes. First is to generate a beam consisting of bunches of electrons, the second is to generate positrons

in the same numbers like were the electrons, since we want to have symmetrical collisions in the collider. The nominal charge for the electron bunch is, as listed above, 3.4 nC and since there is a desire to have at least 50% margin for the positron production, that means 6.8 nC [1]. This however is being subject to exploration in the time when this work is being written and from not yet published works and reports and from regular group meeting, where partial findings are discussed, it seems more likely that the bunch charge for positron production would be way less even with enough margin.

We used more realistic bunch charge of 5.0 nC. In order to preserve the settings of the beam line elements between these two charges as much as possible, we preserve the charge density of the bunch and the only parameter change is the initial beam spot size.

For optimisation, we first need to define the figure of merit which we want to either minimize or maximize. For us there are two most important characteristics to consider, transversal emittance (emittance from now on) and energy spread. As will be explained below, the guiding characteristic for energy spread is emission time, which means we can chose a desired the energy spread value and set the emission time accordingly. From now on, by optimization we mean a process of minimizing the emittance with set energy spread.

4.1 Estimates of the initial bunch characteristics

When we optimise for the geometrical properties of the beam, firstly we need to decide, what distribution of particles to use. Since we are using photoeffect to generate free electrons, the distribution of the electrons will be almost the same as the distribution of the power in the laser pulse. The most basic approach is to consider only Gaussian distribution in all three spatial direction. However this neglects any focusing elements and apertures, which will flatten the distribution in the transversal plane. Distribution of energy in single laser pulse in time will be approximately Gaussian, however we are able to generate pulse lengths several times smaller then needed, which is used for creating more uniform distribution in time [18]. When the short Gaussian pulses are stacked after each other, we create a plateau distribution, which could be defined as sum of subsequent Gaussian distributions.

There is a predefined plateau distribution function in ASTRA, which is used as an approximate result of previously mentioned beam stacking. This distribution has two parametres, length and rise time, where rise time corresponds to deviation of the used Gaussian pulses and length on the number of the pulses and their standard deviation.

This is the reasoning behind optimising for two distinct distribution functions. For the first one we used only Gaussian distribution (in transverse plane the distribution was truncated at double the the standard deviation to take some aperture into account) and is called Gaussian distribution from now on. The second distribution is more sophisticated using the plateau distribution in the longitudinal direction to simulate the beam stacking and radially uniform distribution in the transverse plane, which corresponds to the apertures and beam shaping elements for the laser beam. This will be called flat distribution from now on. For our beam we take the measured values of rise time from SwissFEL [16] since it is our point of reference.

4.1.1 Emission time

Consider a bunch of charged particles uniformly distributed in longitudinal direction with length l and with speed $\beta = 1$ being accelerated (acceleration in this context means adding energy, not increasing speed) by RF travelling wave structure with wave length λ. Assuming that the center of the bunch has zero phase offset from the wave, the acceleration rate is decreasing the further we go from the center. This introduces energy spread to the bunch, which we can calculate as can be seen in Fig. 4.1. The length of the bunch expressed in phase of the RF is $\theta = 2\pi\, Tc/\lambda$. This calculation gives us good estimate of what will the final energy spread be like since it is driven by RF curvature in high energies. However this is the theoretical minimum, realistically effects like space charge will increase the energy spread but also bunch length, which will increase the final energy spread. Here was taken a decision that we aim to have rms energy spread under 0.5% of the average energy and for that 15 ps emission time would be sufficient. This choice of energy spread is arbitrary and can be subject to further change in future developments.

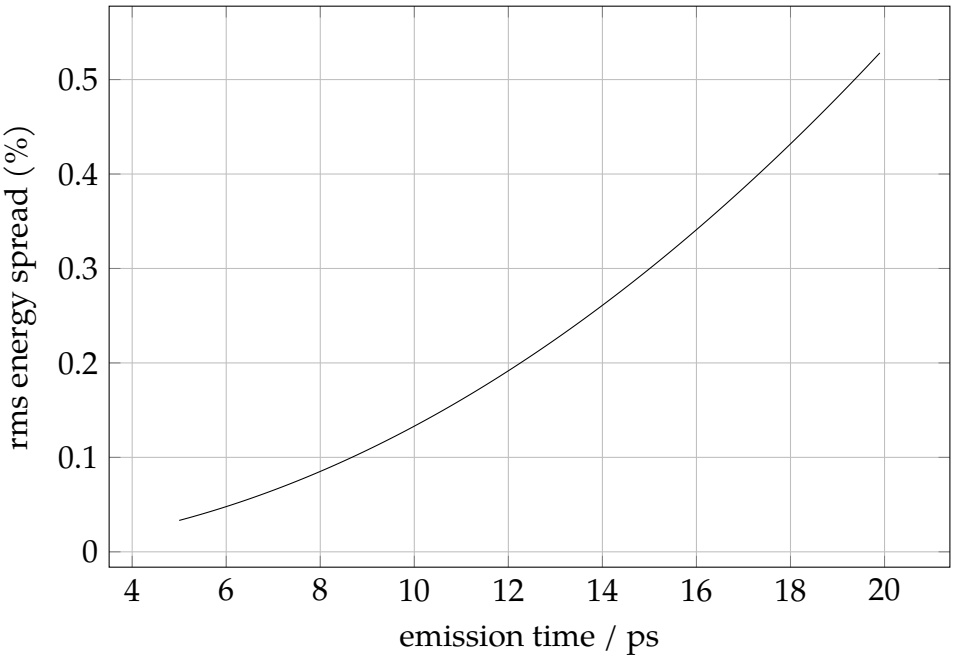

Obrázek 4.1: Dependence of energy spread on emission time

4.1.2 Spot size

The second initial geometrical characteristic of the beam is its radius. Here we can't estimate with analytical calculation since here we need to count with the space charge, which must be calculated numerically. We simulated how bunch of particles with emission time 15 ps, as we decided earlier, would evolve along the beam line taking only the RF gun into account with different initial spot sizes. Here we follow evolution of three main parametres; spot size, bunch length and emittance at distance 0.9 m from the cathode. This distance is arbitrary chosen but near the expected position of the first TWS. As expected the bunch always spread out in all directions. However there is a clear minimum for both spot size and emittance, which as expected means that the lower the initial spot size is the stronger the space charge forces are and so the particles gain more positive radial momentum, increasing the spot size and emittance over time more than larger initial radii.

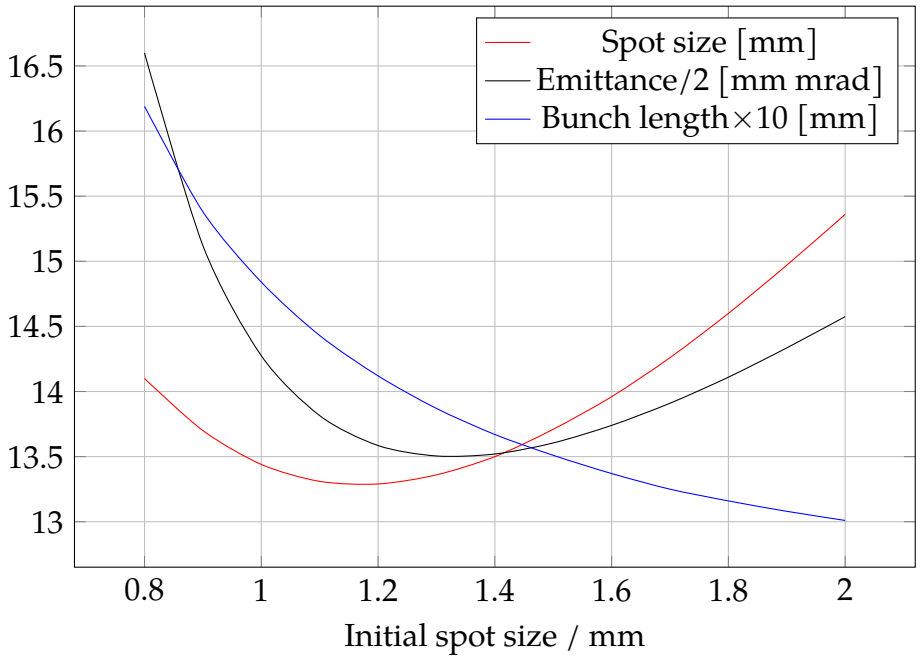

Obrázek 4.2: Dependence of spot size, emittance and bunch length at $z = 0.9$ m distance from the cathode on initial spot size.

The decision was made for the radius to be $r = 1.5$ mm. This is larger radius than the minima of both the spot size and emittance, which means that the space charge forces are less prevalent, and since space charge causes more chaotic behaviour inside the bunch and so the bunch is more stable. Since this is one of the characteristics that are being optimised for, the initial estimate serves only to quicken the process.

4.2 Estimates for the parametres of the structures used

4.2.1 RF-gun

The RF-gun gradient and autophase offset (as explained in Sec. 2.8) of the RF gun will be set to $E_0 = 100\text{MV/m}$ and $\phi_0 = 0$ respectively. These values won't be subject to change during optimisation since we expect the main driving force for emittance growth to be the space

charge and since space charge forces has the most significant effect on the beam in low energy region, the faster we can accelerate the bunch, the lower the emittance and energy spread. If the overall emittance would prove to be too large even after optimising the setup, the gradient could be increased and we could expect betterment of performance. We won't introduce any phase offset since this would be equivalent to decreasing the emission time through bunch compression 2.5.

4.2.2 TWS

For the TWS, only the first structure's parametres are being optimised, since the others have no significant effect on the beam characteristics. We set the maximum gradient of the TWSs to $E_0 = 25\text{MV/m}$ [17] and autophase offset to $\phi_0 = -2^\circ$ in order to decrease correlated energy spread introduced by space charge. Since there is no analytical estimate for the effect of the different gradients of the first TWS on the beam characteristics we set the bounds to 0,25 MV/m. The position of the first TWS is more important than its gradient and we also have some estimate [16] where to expect the optimum position. For the other TWSs, their position is insignificant. The other TWSs are set up in a way, so that the energy at the end of the beam line is around 200 MeV, the reasons are being discussed in Chapter 3.

4.2.3 Solenoid

The initial estimate for the magnetic field of the solenoid is calculated as a field for a given length for which a single particle goes through half of a revolution. If there were no other effects in place, this would focus the beam into its minimal spot size, but with quite large positive radial velocity, but since we are dealing with space charge which defocuses, this proves to be a good initial estimate. The length of the solenoid we are using is $l(\text{FWHM}) = 26\,\text{cm}$ since it isn't uniform we are using the value (the fringe fields won't be considered since we are aiming for initial estimate for subsequent optimisation). We use relation between particle's momentum, field strength and magnetic length $B_0 = \frac{\pi\, p}{l\, e}$ as presented in Sec. 2.7, since we already simulated the bunch to have estimate for initial spot size, we know the momentum the average particle gains in the RF gun is $p = 6.623\,\text{MeV/c}^2$.

So the initial estimate for the solenoid field strength is $B_0 = 0.27\,\mathrm{T}$. We simulated the evolution of the particle bunch along the beam line with previously discussed initial distribution, RF-gun parametres and solenoid with this field strength.

We aim to have the solenoid focusing partially compensated by space charge defocusing, in order for the minimum of the beam spot size to be around the position of the first TWS. If the focusing is compensated by the space charge the minimum of the spot size is wider ($\frac{\partial^2 w}{\partial z^2}$, where w is the spot size width and z is the position, is lower). The wider the minimum the lower is the required precision for the position of the first TWS. The afford mentioned conditions, for the existence of a minimum and width of the minimum, is expressed mathematically in Eq. 4.1.

$$\begin{aligned} g &= \frac{\partial w}{\partial z} = 0 \\ \frac{\partial}{\partial B}&\left(\frac{\partial^2 w}{\partial z^2}\right) \approx 0 \end{aligned} \tag{4.1}$$

To have better initial estimate of the solenoid magnetic field we took the previous argument into account. We have simulated the evolution of the $g = g[B](z)$, as defined in Eq. 4.1. The useful range of solenoid field values is determined from Fig. 4.3 (the green lines $B = (0.22, 0.24)\mathrm{T}$). For the values of the solenoid filed below the estimated range the focusing is not enough to overcome space charge, and above is too strong so the beam reaches its "focal point"(spot size minimum) too fast (high value of second derivative at the minimum).

4.3 Methods of optimisation

We used two different algorithms for optimisation. For the first one we used ASTRA's inbuilt algorithm for optimisation. This however optimised only one "variable"the other characteristics being only "parametres"of the process. Since the inbuilt algorithm is more precise (has more steps), it was used on the characteristic with greatest effect on the beam and without initial estimate, which was the position of the first TWS. The inbuilt optimiser was used across the entire estimated range

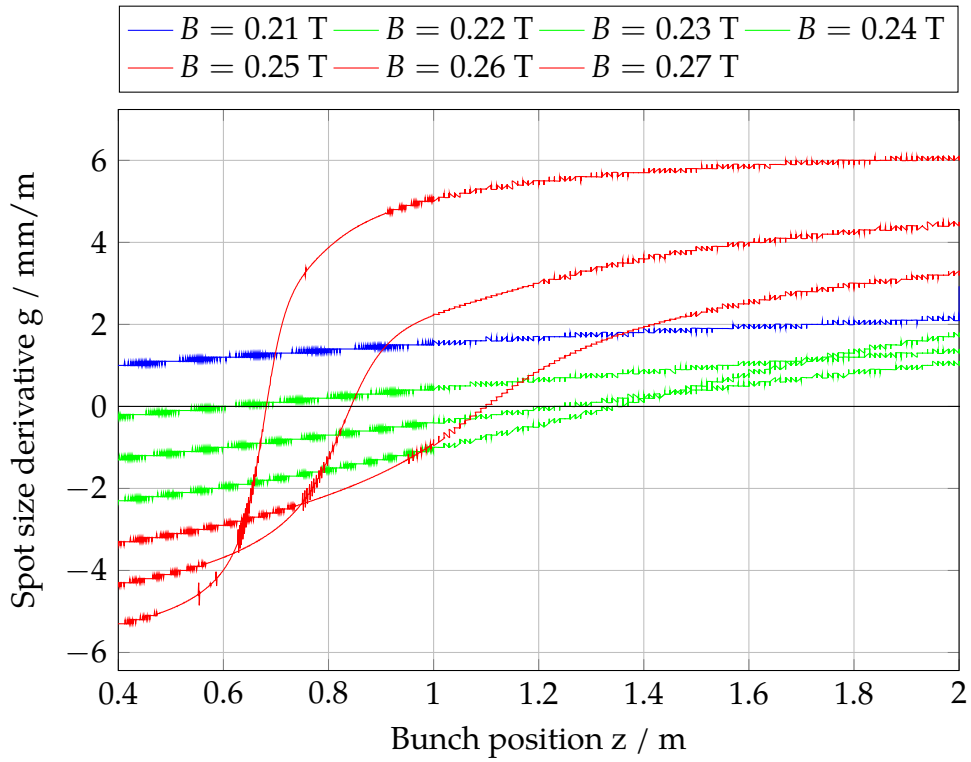

Obrázek 4.3: Spot size derivation as a function of bunch position. The blue function represents solenoid field too weak for focusing and the red ones represent solenoid field too strong for focusing and the green functions represent interval of solenoid field values that can be used for focusing.

of the parametres with N parameter values spaced equidistantly in the range. Since with this approach the computational time increases exponentially with every added parameter, we decided to use only two parametres; solenoid field strength and gradient of the first TWS as the set parametres with position of the first TWS as the variable of the process. The variable was automatically optimised by ASTRA to achieve the lowest emittance. For these simulation we used low resolution set up with larger grid cells and time steps and lower number of makroparticles, then we chose the most interesting runs and did high resolution simulation for them and compared them. This option was used primarily because it gave us overview of what is happening

to the characteristics in the previously determined range. This shall be called the "manual"algorithm from now on.

The second approach was to use simplex algorithm developed by Bettoni [16], where we used the result from the previous algorithm as an initial estimate and let the code optimise. We also added as an optimisable parameter the initial spot size. This shall be called the "automatic"algorithm from now on.

4.4 Results

4.4.1 Optimisation for electron production and flat distribution and comparison of optimisation algorithms

At first we need to assess which of the algorithms to use. To do that we compare their lowest achieved emittance and complexity of usage. It is expected, that the automatic algorithm performs better than the manual one, however the manual algorithm is much less vulnerable to produce incorrect results and doesn't need to be changed for different distributions. We assess the different performances of these two algorithms in this section. In order to use similar set up for the structures as with 5.0 nC beam, we decreased the estimate of the initial spot size so that the charge density is the same for both charges.

Figures in Tab. 4.3 show us that there isn't significant change in how the characteristics evolve in time, merely a change of the actual values. The only notable difference being the distribution, where automatic algorithm is better able to preserve the initial distributions. Since this is very early study, the difference in the final emittance and energy spread are insignificant between those two algorithms, so it is beneficial to use the manual algorithm for first round of optimisations giving similar results with less time spend. Since the automatic algorithm can optimise for not only the maximum fields but also for the shape of the field from certain selection, once there are field distributions to chose from, the automatic algorithm is to be used instead of the manual.

Tabulka 4.2: The initial beam parametres and structure parametres (left). The main beam characteristics at distance 15 m from the emitter (the end of the injector).

	manual	automatic
Bunch charge	3.4 nC	3.4 nC
Initial spot size	1.23 mm	1.232 mm
Emission time [FWHM]	15 ps	15 ps
Solenoid magnetic field	0.225 T	0.2413 T
Cavity gradient	15 MV/m	16.2 MV/m
Cavity position	1.47 m	1.068 m

	manual	automatic
Transversal emittance	3.08 mrad mm	1.94 mrad mm
Energy spread	642 keV	703 keV
Average energy	202 MeV	206 MeV
Beam size	1.01 mm	1.05 mm
Bunch length	1.31 mm	1.36 mm

4.4.2 Optimisation for positron production with flat distribution and details of the manual algorithm

Here we optimised for the positron production total charge (5.0 nC) and flat particle distribution, in order to get maximum performance without any restrictions for the optimised parameters.

From these simulations were chosen (green mark) two runs, since they have similarly high performance, with different parameter set up. First is higher magnetic field and lower electric gradient and the other is opposite.

As we can see from the figures in Tab. 4.6, the evolution of beam characteristics is in both cases very similar. The bunch length evolve almost the same which is expected since the initial characteristics and RF-gun electric field are set up the same. Since most of the energy spread is induced by RF curvature at the TWS, the energy spread is also expected to be almost identical relative its respective average energy. The difference in the transversal emittance is insignificant in regions where there is no TWS electric field, in case #1 there is observably more noise when there is electrical field. However these are low relatively to final emittance.

Tabulka 4.3: Evolution of critical characteristics of the beam as it travels through the beam line for two different set of parametres and the particle distributions at 15 m distance from the cathode

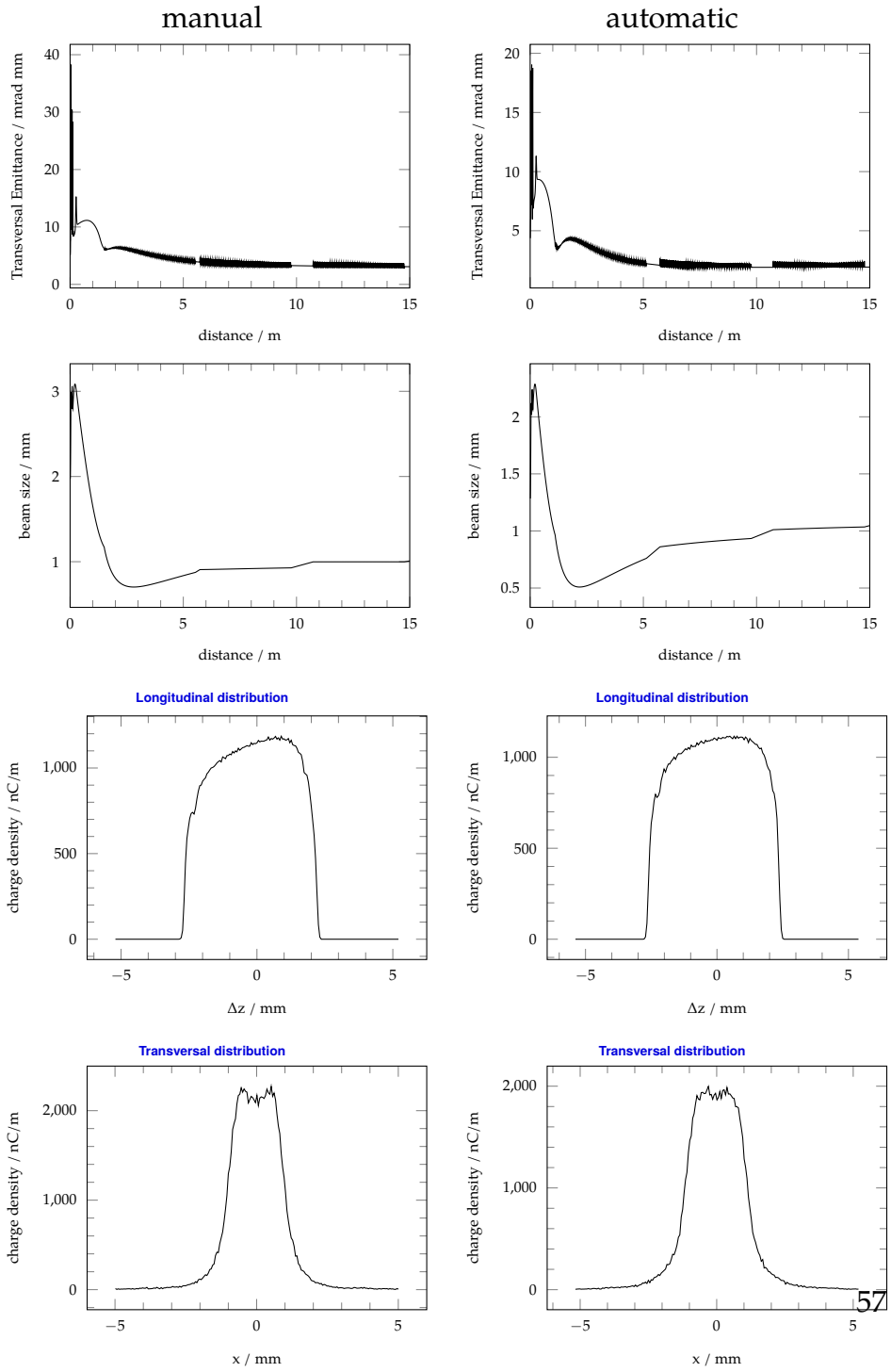

Tabulka 4.4: Manual optimisation method. Cells show the projected transversal emittance [mm mrad] / position of the first cavity [m].

B_{sol}[T]\E_{cav}[MV/m]	10	15	20	25
0.21	10.5/0.85	11.5/0.50	12.5/0.50	
0.22	6.6/1.28	6.6/1.57	6.5/1.79	6.1/1.89
0.23	7.3/0.80	6.0/1.21	5.4/1.29	5.2/1.36
0.24	5.0/1.09	3.9/1.09	4.5/1.16	6.0/1.23

Tabulka 4.5: Parametres of the two simulations being done in higher precision.

	#1	#2
Bunch charge	5.0 nC	5.0 nC
Initial spot size	1.5 mm	1.5 mm
Emission time [FWHM]	15 ps	15 ps
Solenoid magnetic field	0.24 T	0.23 T
Cavity gradient	15 MV/m	25 MV/m
Cavity position	1.09 m	1.36 m

From figures in Tab. 4.7 we can see that the longitudinal and momentum distributions are almost identical. There are three clearly visible peaks in the momentum distributions. These probably are the center with highest momentum and particle density, head with lower momentum because of bunch compression and tail with lowest momentum and density due to space charge effects. The appearance of the secondary peaks of head and tail is to be expected since those are regions with sudden decrease of particle density (initial distribution was plateau in long. direction). Interestingly these secondary peaks appear to be vanishing with increased momentum (the average momentum of the #2 case is higher than the #1 case). It is also worth noting that the longitudinal and transversal distribution are partially preserved from their initial states, in longitudinal direction more. Also for the #1 case, the transversal distribution is preserved more than for the #2 case.

Tabulka 4.6: Evolution of critical characteristics of the beam as it travels through the beam line for two different set of parametres

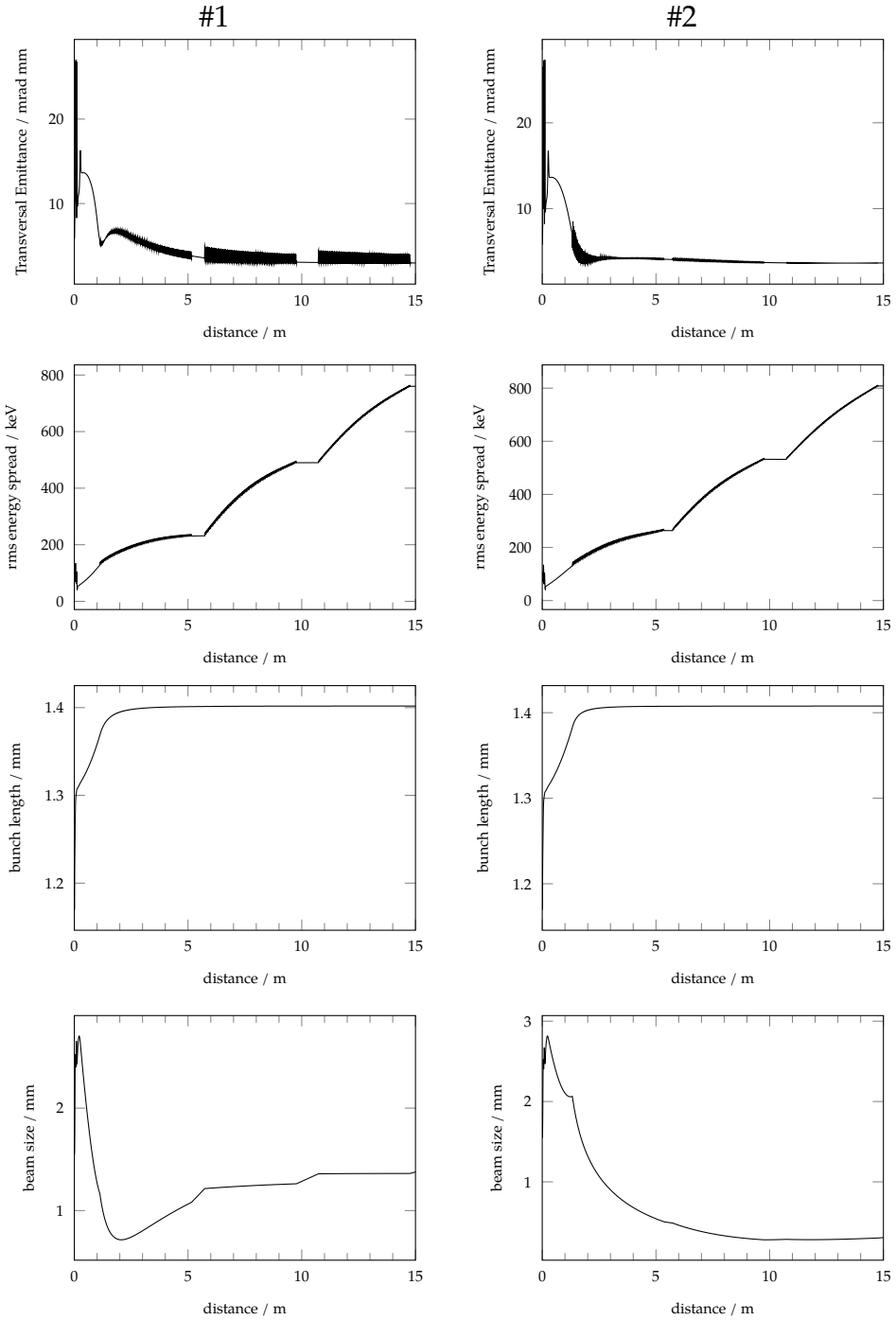

Tabulka 4.7: The particle distributions at 15 m distance from the cathode.

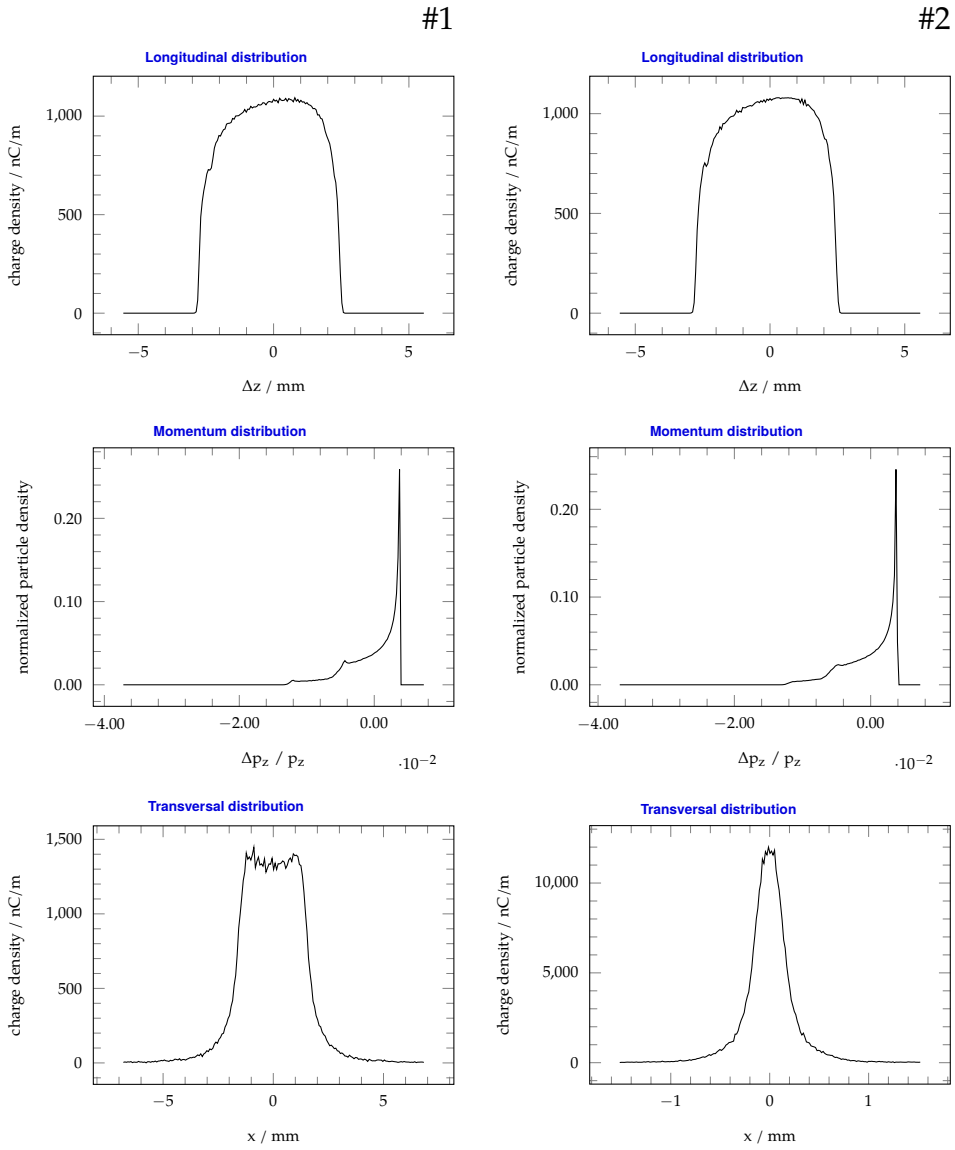

Tabulka 4.8: Main beam characteristics at 15 m distance from the emitter.

	#1	#2
Transversal emittance	2.96 mrad mm	4.05 mrad mm
Energy spread	760 keV	867 keV
Average energy	202 MeV	232 MeV
Beam size	1.38 mm	0.63 mm
Bunch length	1.40 mm	1.41 mm

4.4.3 Optimising with engineering restrictions

Since both of these different charges will be done on a single device during single operation we need to add additional restrictions, meaning there are several parametres that can't be changed during operation, such as positions of the structures along the beam line and gradient of the structures, since it requires comparably long time to decrease or increase the field in the whole structure. As stated before the higher total charge bunch is made for positron production, so optimising for that charge isn't that crucial so we take the results from the automatic algorithm in Sec. 4.4.1 and optimise the solenoid magnetic field strength.

Tabulka 4.9: The initial parametres of the beam and the parametres of the structures along the beam line. And the main beam characteristics at 15 m distance.

Bunch charge	5.0 nC
Initial spot size	1.5 mm
Emission time [FWHM]	15 ps
Solenoid magnetic field	0.239 T
Cavity gradient	16.2 MV/m
Cavity position	1.068 m
Transversal emittance	2.80 mrad mm
Energy spread	760 keV
Average energy	206 MeV
Beam size	1.10 mm
Bunch length	1.40 mm

From Tab. 4.10 we can see that even with restriction we were able to get the characteristics below original optimum. This means that we can easily change between the operations with different bunch charges by changing beams spot size, to preserve the charge density, and the solenoid magnetic field strength. This means that any further optimisation can be done solely for the nominal charge (3.4 nC) since even after charge increase it remains being well optimised. We omitted presenting the evolution figures since it is expected that they are similar to the nominal charge case.

4.4.4 Results of beam with Gaussian distribution

Changing the charge distribution in the beam fundamentally changes its behaviour in phase space. However we expect the evolution of the beam characteristics to be similar to the previous cases. Since this distribution is done only for comparison and to assess the lowest optimised case we optimised only for the nominal total charge.

Tabulka 4.10: Initial beam parametres and structure parametres. Main beam characteristics at 15 m distance from the emitter.

Bunch charge	3.4 nC
Initial spot size [rms]	0.80 mm
Emission time [rms]	4.5 ps
Solenoid magnetic field	0.245 T
Cavity gradient	10 MV/m
Cavity position	0.78 m
Transversal emittance	8.26 mrad mm
Energy spread	1102 keV
Average energy	187 MeV
Beam size	1.04 mm
Bunch length	1.61 mm

As expected the final emittance and energy spread values are higher than with the flat distribution by a factor around three. The longitudinal distribution is very well preserved, the transversal one, on the other hand, creates two distinct parts, center peak where most of the charge is concentrated and sparsely populated outer ring. In

Tabulka 4.11: The particle distributions at 15 m distance from the cathode with initial Gaussian distribution

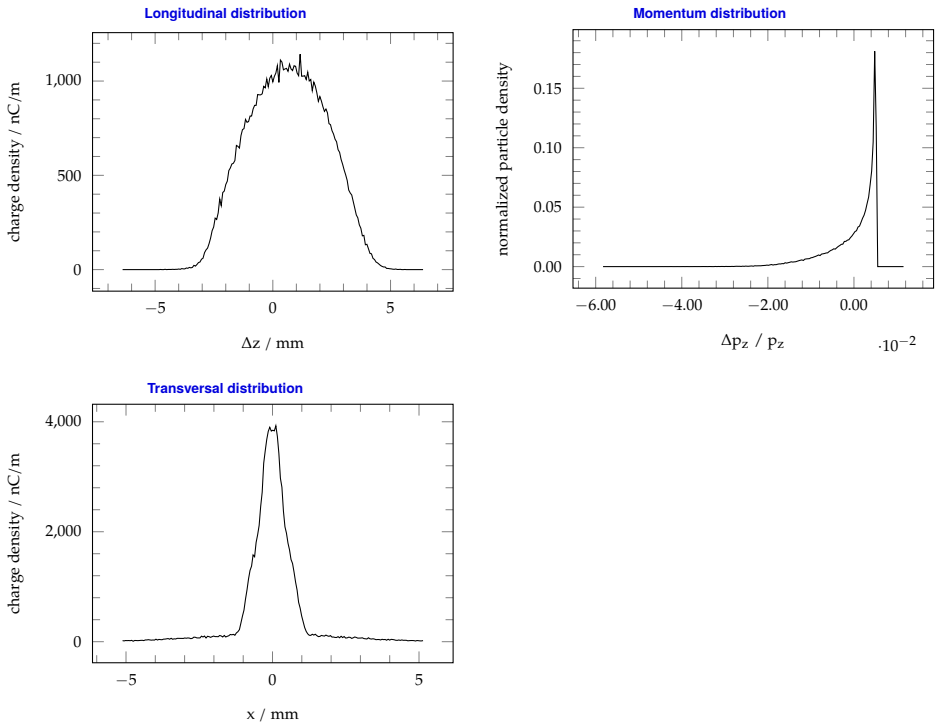

the momentum distribution we can't see any distinct peaks other than the central one. This is expected since the distribution is smooth in comparison with the plateau one.

5 Conclusion and summary

The photoinjector we examined was proven to be a viable option for the FCC-ee as a electron source and the first part of the electron injector chain.

The options for cathode emitter materials were also examined and it was concluded, that currently available PEA semiconductor cathodes are well able to generate time structure required, since its response time is of an order lower than the required bunch length, and are able to withstand the power required to generate the required charge. For the metal cathode emitter option there is no definitive conclusion, since the required power density, the emiter needs to withstand, is near the ablation threshold, and needs to be studied more thoroughly in subsequent works. The concrete material and operation parametres, such as pressure, temperature etc. are to be determined in subsequent works and was out of the scope of this work.

We studied the particle behaviour traveling in bunches in accelerating structures and under the influence of internal and external electric and magnetic forces. With this knowledge we used emittance as a physical quantity to assess performance of the injector.

By examination of two previously existing optimization methods, we give overview of advantages for both and how they would be best used. The manual algorithm is best used in assessing some first estimates and feasibility of the design. The automatic algorithm is best used in optimization of the design chosen in previous step.

The results of our optimization are available and are examined in greater detail in this work to give comprehensive overview for other research teams working on FCC-ee injector facilities. We have examined three different configurations, uniform distribution with nominal bunch charge 3.4 nC, uniform distribution with produciton bunch charge 5.0 nC and Gaussian distribution with nominal charge. The uniform distribution is the best case scenario studied, so its transversal emittance of $\varepsilon = 1.94\,\text{mm mrad}$ is the lowest theoretical minimum for this setup. The Gaussian distribution is the worst case scenario studied and its optimised emittance of $\varepsilon = 8.26\,\text{mm mrad}$. These results are well in the range for the collider to perform well and are to be used

in subsequent works of other teams designing the facilities after the injector.

The concrete initial distributions are to be determined once the laser power distribution is known and the optical focusing elements are added, which is to be determined in subsequent works. Also other requirements will arise as studies on facilities down the beam line oare finished that will need to be counted in.

A Electron emission process

In this Appendix, we shall describe details of three step emission process as described in [3].

A.1 Excitation

A laser is most often used as a source of the photon flux, due to its inherent attribute, that it produces a photon beam with very low bandwidth, so we can, for the most cases, approximate a single wavelength being emitted. Also the beam have very high coherence and very high power density, both in radial and temporal distributions.
Now we shall describe a mechanism of the photon absorption in clean (the surface isn't modified) metals. Firstly we define the rate per unit area at which electrons are excited between energies E and $E + \mathrm{d}E$ in a layer $\mathrm{d}x$ located a distance x from the surface as

$$G(E, x)\mathrm{d}E\mathrm{d}x = G_0 \mathrm{d}E e^{-\alpha x}\mathrm{d}x, \tag{A.1}$$

where α is the absorption rate and G_0 is defined as

$$G_0 = n_p \alpha'_\nu, \tag{A.2}$$

where n_p is the photon flux at frequency ν and α'_ν is defined through the absorption coeficient as

$$\alpha(\nu) = \int_0^\infty \alpha'_\nu(E)\mathrm{d}E, \tag{A.3}$$

in order that the $\alpha'_\nu(E)$ corresponds to part of $\alpha(\nu)$ due to electronic transitions between states E and $E + \mathrm{d}E$. Assume that $N_T(E, E_0, \nu)$ is a probability that transition occurs with initial energy state E_0 and final energy state E in a presence of electromagnetic wave with frequency ν per second per volume unit. Since the conservation of energy requires that $E = E_0 + h\nu$, the N_T in not independent function of both E and E_0. The power absorbed per volume unit can be written as

$$P = h\nu \int_0^\infty N_T(E, E_0, \nu)\mathrm{d}E, \tag{A.4}$$

and we know that the conductivity is defined as

$$P = \frac{1}{2}\mathcal{E}^2\sigma, \tag{A.5}$$

and the the absorption coefficient

$$\alpha(\nu) = \frac{\sigma(\nu)}{n(\nu)c\varepsilon_0}, \tag{A.6}$$

where n is the refraction index and ε_0 is permitivity of free space. By using eq. A.5, eq. A.4 and eq. A.6 we derive

$$\alpha(\nu) = \frac{2h\nu}{n(\nu)c\varepsilon_0\mathcal{E}^2}\int_0^\infty N_T(E, E_0, \nu)\mathrm{d}E. \tag{A.7}$$

Comparing eq. A.6 and eq. A.3

$$\alpha'_\nu(E) = \frac{2h\nu}{n(\nu)c\varepsilon_0\mathcal{E}^2}N_T(E, E_0, \nu). \tag{A.8}$$

We can now express $G(E, x)dEdx$ by material constants, the absorption coefficient α_ν, the refraction index $n(\nu)$ and $N_T(E, E_0, \nu)$, which we can determine by using first or/and second order perturbation theory if the wave functions in the solid are known.

$$G(E, x)\mathrm{d}E\mathrm{d}x = n_p\frac{2h\nu}{n(\nu)c\varepsilon_0\mathcal{E}^2}N_T(E, E_0, \nu)\mathrm{d}Ee^{-\alpha x}\mathrm{d}x, \tag{A.9}$$

A.2 Emission

Once we know the transition probability of electron with initial energy E_0 and final energy $E = E_0 + h\nu$, we need to determine the behaviour of such electron and the probability that such electron will escape into the vacuum. Consider an electron excited to some energy E with momentum $\mathbf{p}$ and some distance from surface x as shown in Fig. A.1. In order for the electron to leave the solid its momentum component perpendicular to the surface of the solid must be above some momentum threshold.

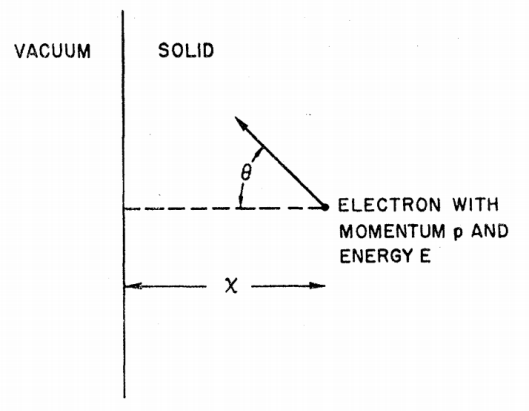

Obrázek A.1: Electron momentum in solid after absorbing photon with energy $h\nu$

The probability of the electron to reach the surface with required momentum and without being inelastically scattered is

$$p_{\text{esc}} = \frac{1}{2}\int_{p_c/p}^{1} e^{-x/zl}\mathrm{d}z \text{ for } p > p_c, \tag{A.10}$$

otherwise $p_{\text{esc}} = 0$, where $z = \cos\theta$, where θ is the angle between the electron momentum and the direction perpendicular to the surface, x is the distance of the electron from the surface and l is mean free path of the electron in a solid.

There are two mechanisms of inelastic collision, by which the electron loses its energy. First is electron-electron scattering, contributing most of the loss of energy of the electron in the metal, where as much as half of the energy is given to the other electron. If this happens, when the electron energy is close to the work function, neither of those electrons will escape. If the energy is above twice the threshold, both of those electron will be emitted if they don't suffer any additional scattering. The other mechanism is electron-phonon scattering, by which on the other hand the energy loss is very small and for metals can be neglected, however for semiconductors, this is not the case and will be discussed in this section.

For a semiconductor the situation is a bit more complicated since there is a band gap between valence and conductive bands. So in order for the electron to be emitted from the semiconductor cathode, the energy of the photon can be divided into two parts, the band energy and electron affinity. The electron affinity can vary a lot depending on specific circumstances. For cathodes however, only two options make sense to use being low electron affinity in comparison with its band gap energy found for example in $CsTe_3$ or negative electron affinity made for example by doping surface of GaAs with oxygen.

With electron affinity being lower than the band gap, if the electron is excited so it can escape the cathode, it doesn't bear enough energy to excite another electron above band gap so there is no possibility of e-e scattering, so the only mechanism remaining is the e-p scattering and since the electron loses only small portion of its energy by it, even electrons from much deeper in the bulk of the material can be excited. For negative electron affinity cathodes, the travel distance is virtually limitless, but since the electrons are in the lowest state in the conductive band, they travel by diffusion explained by [19] and [20].

For both metal and semiconductor the behaviour during the third step, being the actual emission, is the same. When the electron is emitted, it gains velocity with speed depending on the energy the electron has and with anisotropic distribution of momentum due to the requirement on the perpendicular part, which is being consumed by the emission. So the rms of momentum parallel to the surface remains the same as it was in the cathode, but the rms of the perpendicular momentum is $p_{p,out} = p_{p,in} - \sqrt{2m\Phi}$.

B Solutions of RF cavity electromagnetic fields

B.1 Standing wave cavity

The main idea for the standing wave cavity is that the frequency of the rf wave in the cavity is synchronised with the revolution frequency of the beam, so the beam is only affected by a positive electric field in order to be accelerated. Let's suppose, that we have a circular accelerator with constant radius ρ and beam velocity β. Than the cavity electric frequency is equal to the revolution frequency of the beam

$$\omega_{RF} = \frac{\beta c}{\rho}, \tag{B.1}$$

As for the actual design of the cavity goes, we can simply assume a pillbox with radius R and width H as an approximation as shown in Fig. B.1. From the Maxwell eq.s we derive a general solutions for the pillbox cavity for electric and magnetic field, assuming propagation through free space

$$\begin{aligned} \Delta\mathcal{E}(x,y,z) + \frac{\omega^2}{c^2}\frac{\partial^2\mathcal{E}(x,y,z)}{\partial t^2} &= 0 \\ \Delta\mathcal{H}(x,y,z) + \frac{\omega^2}{c^2}\frac{\partial^2\mathcal{H}(x,y,z)}{\partial t^2} &= 0, \end{aligned} \tag{B.2}$$

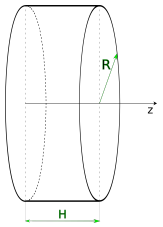

Obrázek B.1: Pillbox cavity.

where $\mathcal{E}$, resp. $\mathcal{H}$ is electric, resp. magnetic, intensity. We assume $\rho = 0 \wedge \mathbf{j} = \mathbf{0}$ and the walls of the cavity conduct without losses. Since both of the Eq. B.2 are bound together by Maxwell equations, we only take solutions satisfying both of them.

$$\mathbf{E}(t,x,y,z) = \mathcal{E}(x,y,z)e^{-i\omega t} \tag{B.3}$$

The pillbox is giving us the boundary conditions

$$\mathcal{E}(R,\varphi,z) = \mathcal{E}(r,\varphi,0) = \mathcal{E}(r,\varphi,H) = \mathbf{0} \tag{B.4}$$

for which we can solve the Eq. B.3 by separation of variables. There are two very distinct general solutions, which we call $TE_{m,n,l}$ (transverse electric) and $TM_{m,n,l}$ (transverse magnetic) modes, where m, n, l are integers describing each solution. Since only the TM modes have non-zero longitudinal electric component, we neglect the TE modes (they are needed to describe the exact transversal motion). The solutions for TM modes are

$$\begin{aligned}
E_r &= -E_0 \frac{k_z}{k_r} J_n'(k_r r) \cos n\theta \sin k_z z \, e^{-i\omega t} \\
E_\theta &= E_0 \frac{n k_z}{k_r^2 r} J_n(k_r r) \sin n\theta \sin k_z z \, e^{-i\omega t} \\
E_z &= E_0 \, J_n(k_r r) \cos n\theta \cos k_z z \, e^{-i\omega t} \\
B_r &= iE_0 \frac{n\omega}{c^2 k_r^2 r} J_n(k_r r) \sin n\theta \cos k_z z \, e^{-i\omega t} \\
B_\theta &= iE_0 \frac{\omega}{c^2 k_r} J_n'(k_r r) \cos n\theta \cos k_z z \, e^{-i\omega t} \\
B_z &= 0
\end{aligned} \tag{B.5}$$

where k_r and k_z

$$k_r = \frac{p_{mn}}{R}, \; k_z = \frac{\pi l}{H}, \tag{B.6}$$

are radial and longitudinal wave numbers respectively The coefficient p_{mn} is the m root of the n order Bessel function $J_n(x)$ and so the integers m, n, l are representing radial, azimuthal and longitudinal modes respectively. The frequency corresponding to each mode is determined through dispersion relation

$$\omega^2 = \frac{c^2}{k^2}, \tag{B.7}$$

where k is the magnitude of the wave vector

$$k^2 = k_r^2 + k_z^2. \tag{B.8}$$

The frequency expressed for each mode TM_{mnl} is

$$\omega_{mnl} = c\sqrt{\left(\frac{p_{mn}}{R}\right)^2 + \left(\frac{\pi l}{H}\right)^2}. \tag{B.9}$$

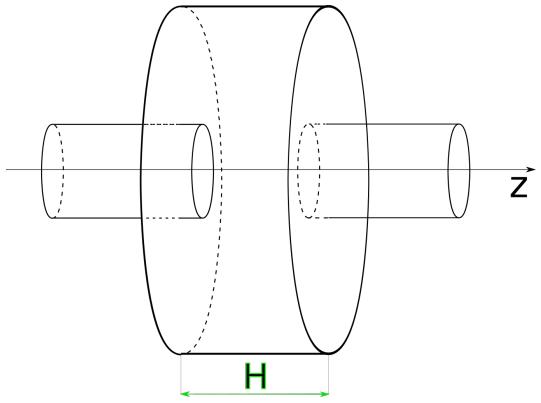

h!

Obrázek B.2: Perturbed cavity

Since the cavity has non-zero length and the velocity of the beam is capped at c there is non-zero transit time factor τ and so the phase of the cavity also change as

$$\varphi_f = \varphi_i + \omega\tau = \varphi_i + \omega\frac{H}{\beta c}. \tag{B.10}$$

Because of this phenomenon, the lower the frequency of the standing wave cavity is, the better is the approximation that the beam travels through the structure with constant phase. We also have to consider the perturbation of the solutions of the equation by the beam pipe that does through the cavity as shown in Fig. B.2.

B.1.1 Solutions for simple waveguide

If we take axisymetrical cylindrical waveguide with coordination system r, θ, z and the propagation is in z direction and we take the TM_{01} mode, since this is the base accelerating mode we get

$$\begin{aligned} E_z &= E_0 J_0(k_c r) e^{i(\omega t - \beta z)} \\ E_r &= iE_0\sqrt{1-(\omega_c/\omega)^2} J_1(k_c r) e^{i(\omega t - \beta z)} \\ B_\theta &= i\mu_0 E_0 J_1(k_c r) e^{i(\omega t - \beta z)} \end{aligned} \tag{B.11}$$

where J_0 and J_1 are Bessel functions of first kind, $\omega_c = ck_c$ is the cut off frequency

$$\omega_c = c\frac{p_{01}}{R} \tag{B.12}$$

where p_{01} is as mentioned above the root of corresponding Bessel function. The electromagnetic wave in a waveguide oscillate with cutoff frequency, when the wave number in the propagation direction k_z is equal to zero. The same result can be obtained using the results of the pillbox cavity assuming the length of the cavity H goes to infinity. The last variable in Eq. B.11 is propagation constant $\beta = \omega/v_{ph}$, $\beta^2 = k^2 - k_c^2$, $k = \omega/c$ so

$$\frac{\omega^2}{v_p^2} = \frac{\omega^2 - \omega_c^2}{c^2} \;\Rightarrow\; v_{ph} = c\frac{1}{\sqrt{1-(\omega_c/\omega)^2}}. \tag{B.13}$$

The propagation constant (and phase velocity) must be real in order for these solutions to exist. This mandates that the phase velocity is always greater than or equal to c. We can rearrange the above equation into one that corresponds to a hyperbola

$$\begin{aligned} &\left(\frac{\omega}{c}\right)^2 - \beta^2 = \left(\frac{\omega_c}{c}\right)^2 \\ &\Rightarrow v_{ph} = \frac{\omega}{\beta} = \sqrt{\frac{\omega_c^2}{\beta^2} + c^2} \\ &\Rightarrow v_g = \frac{d\omega}{d\beta} = \frac{c\beta}{\sqrt{\frac{\omega_c^2}{c^2} + \beta^2}} = \frac{c^2}{v_{ph}} \end{aligned} \tag{B.14}$$

Since the particles we are trying to accelerate will never have velocity greater than c, simple wave guide won't work as an accelerator structure. For a more thorough analysis see [21].

B.1.2 Periodically loaded structures

If we take the cylindrical waveguide and put small radial obstacles (irises) there periodically, than we can assume that it will have negligible effect on propagation (since the obstacles are small) of every frequency

except those for which the spacing between the apertures is equal to $\lambda/2$ or a multiple of that, where the successive reflections from each obstacle add up to create series of stopbands separated by passbands and the smaller the apertures get the smaller the passbands and wider the stopbands are. This forces the above mentioned hyperbola to fold around a certain frequency f_0 which is the frequency of one mode of corresponding pillbox cavity, which has length in z direction same as is the spacing between the irises. The field configuration we get from periodically loaded structure has periodic boundary conditions, so we can analyze space harmonics using Fourier series

$$E_z = \sum_{n=-\infty}^{n=\infty} a_n J_0(k_{rn} r) e^{i(\omega t - \beta_n z)} \tag{B.15}$$

where $k_{rn}^2 = k^2 - \beta_n^2$, $\beta_n = \beta_0 + 2\pi n/d$ where β_0 is the propagation constant of the fundamental space harmonic.

We should also address the other two non-zero components of the fundamental mode E_r, B_θ. Since we want the maximum accelerating field, we ought to chose the phase of the cavity seen by the particles to be close to zero, and since these two components are phase shifted by $\pi/2$ their contribution to the particle motion is not significant but still needs to be counted in when working with long structures with high gradients, where the integrated effect on the particle motion could prove to be strong.

B.2 Design parametres

In this section we will define and discuss basic design parametres, which affect the power efficiency, the amplitude of wave modes and other, that are needed for operation of the accelerator. Since in this thesis, the actual operation of the accelerator won't be dealt with, we only briefly mention the most important ones.

B.2.1 Frequency

From historical and practical point of view, there are certain microwave frequencies that are used for cavities more often others and are called by the name of the microwave band, to which they belong. For our purposes we need to discuss three bands, L, S and C. For each there are two frequencies, one is European and one American. For S band the frequency is chosen so the wavelength is 10 cm and 4 inches for the European and American respectively. The other bands are harmonics of that, so the wavelength of L band is 20 cm and of C band is 5 cm.

The reason that we have chosen the S band for our injector is that it was already successfully implemented in the SwissFEL in PSI. Also we can't go to the above frequency since we would need much (2 times) lower bunch length to preserve energy spread, which would heavily increase transversal emittance. We would also need to decrease the aperture if would would want to preserve the power characteristics, discussed below, which would increase the wakefield effects [22] and since we would have lower bunch length, there is serious possibility that the transversal dimensions would exceed the aperture, so we would need to increase the aperture, which would worsen the power characteristics like filling time and to have the same electric gradient, we would need to increase power input. The major reason into considering C band is that the optimised cavities can have more gradient since as mentioned above, the maximum gradient before electrical breakdown scales with $\sqrt{f}$.

B.2.2 Geometrical dimensions

The basic dimensions of the cavity determine the frequency of all the modes, not only the fundamental. This is why when designing a cavity the radius is determined by the fundamental mode and the height by the first order mode. We want this mode to be TM_{011} and not TM_{020}

this means that

$$H > \frac{c}{2f}\sqrt{\frac{p_{01}^2}{p_{02}^2 - p_{01}^2}} \qquad (B.16)$$
$$H > \frac{\lambda}{4}$$

where f and λ are frequency and wavelength of the fundamental mode, p are roots of the Bessel function. The other thing is that we want the modes to be as spaced as possible in the frequency domain, which means that the height is to be $H = \lambda/2$.

There is also the aperture dimension, however they are primarily involved in energy spread and storage, they will be discussed below.

B.2.3 Shunt impedance and Quality factor

Shunt impedance is defined as

$$r_0 = -\frac{E_{0z}^2}{\mathrm{d}P/\mathrm{d}z} \qquad (B.17)$$

and can be understood as a parameter measuring how much gradient the cavity can create with given power. The "unloaded"quality factor Q is defined as

$$Q = -\frac{\omega w}{\mathrm{d}P/\mathrm{d}z}, \qquad (B.18)$$

where w is the energy density. The "loaded"Q also takes into account loses due to coupling to external waveguides and beam loading. The quality factor measures the energy stored per unit length with given power input. These two parametres together create third one, the so called "r upon Q"defined from the previous equations

$$\frac{r_0}{Q} = \frac{E_{0z}^2}{\omega w} \qquad (B.19)$$

The last parameter here is equal to the group velocity. As is known, group velocity can be equated in most of times to energy flow. Though not true in general, this works for RF cavities. This determines the

"filling time"of RF cavity, which can be defined as simply as $t_f = l/v_g$ where l is the length of the cavity. This puts some constraint on the cavity's length but for fresh cavity filled with energy this doesn't matter so is only important for multibunch operation where the bunches at the head of the train can extract the energy from the cavity and if the filling time is to high and stored energy to low, the dynamics of the each bunch will be different which is undesirable. These parametres as can be seen from their definitions are mostly involved in dealing with connection of power input, stored energy and electrical gradient. Although they are very important from the cavity design and engineering point of view, these parametres don't affect the beam dynamics and so they won't be considered in any greater detail. More information can be given to reader in [8].

C Solenoid focusing

Let's assume a coordinate system x, y, z (horizontal, vertical and longitudinal directions respectively) and let the beam travel along the z coordinate. The solenoid field has only the z component and has the length L. Now we can rewrite the equations for the field components with Taylor series

$$\begin{aligned} B_z(r,z) &= B(z) - \frac{r^2}{4}B''(z) + [HOC] \\ B_r(r,z) &= -\frac{r}{2}B'(z) + \frac{r^3}{16}B'''(z) + [HOC] \end{aligned} \tag{C.1}$$

which is the direct result of equation $\nabla \mathbf{B} = 0$ and our previous definition of the magnetic field. We divide space into three regions. First is before the solenoid, third is after the solenoid and second is the solenoid. We assume magnetic field at the axis as

$$B(z) = \begin{cases} B_0 & \text{if } z \in \langle 0, l \rangle, \\ 0 & \text{otherwise,} \end{cases} \tag{C.2}$$

so $B(z)$ abruptly drops at the longitudinal boundaries, i.e. there are no fringe fields. The first order approximation that satisfies the equations C.1 is

$$\begin{aligned} B_z(r,z) &= B_0 \left[H(z) - H(z-L)\right] \\ B_r(r,z) &= -\frac{r}{2}B_0 \left[\delta(z) - \delta(z-L)\right], \end{aligned} \tag{C.3}$$

where $H(z)$ is the Heaviside step function and $\delta(z)$ is the Dirac delta distribution.
We assume that the beam have zero transversal components of momentum $p_x = 0$ and $p_y = 0$, so the change in momentum of the particles of the beam upon entering the solenoid is

$$\begin{aligned} \frac{\mathrm{d}p_\theta}{\mathrm{d}t} &= \frac{\mathrm{d}p_\theta}{\mathrm{d}z}\frac{\mathrm{d}z}{\mathrm{d}t} = -eB_r v_z \\ \Delta p_\theta &= e\,\frac{r}{2}B_0 \\ \Delta v_\theta &= r_0\,\frac{eB_0}{2m\gamma} \end{aligned} \tag{C.4}$$

The cyclotron frequency is defined as $\omega_c \equiv eB_0/m\gamma$ and here we define the Lamour frequency $\omega_L \equiv eB_0/2m\gamma$ which will be later used to describe the particle trajectory.

We take the paraxial approximation so that the angular momentum in the solenoid is still negligible part of the total momentum $|p| \simeq p_z$. Now we have non-zero component of momentum perpendicular to the magnetic field, so the Lorentz force acting upon the particles is always centrifugal so the particles are performing cyclic movement in the transversal plane. The radius of the circle is determined by equating centrifugal force with the Lorentz force

$$\begin{aligned} \gamma m \frac{v_\theta^2}{R} &= e v_\theta B_0 \\ R = \frac{\gamma m v_\theta}{eB_0} &= \frac{\gamma m \dfrac{eB_0}{2m\gamma} r_0}{eB_0} \\ R &= \frac{r_0}{2} \end{aligned} \tag{C.5}$$

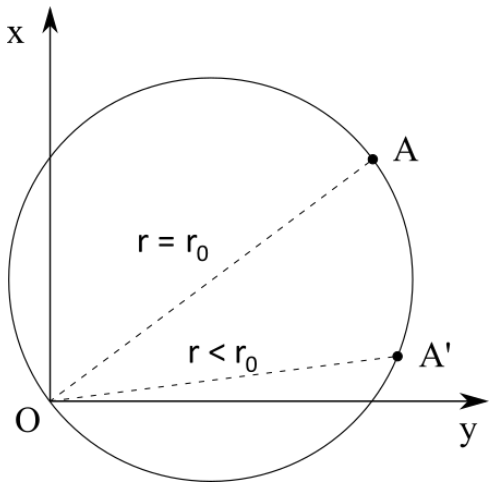

Obrázek C.1: The particle trajectory upon entering the solenoid field.

From Eq. C.5 is obvious that each particle's trajectory is circle touching the axis, with diameter equal to the distance of the particle from the axis upon entering the solenoid as shown in Fig. C.1. Now

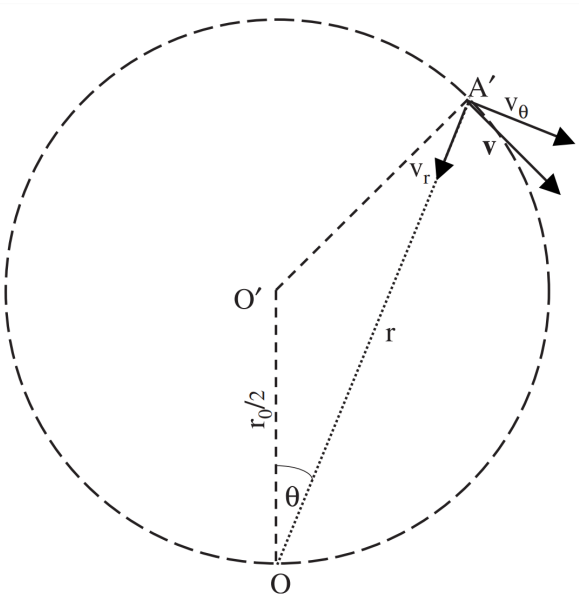

Obrázek C.2: Decomposition of the particle velocity into radial and angular components with respect to the solenoid axis.

let's discuss the particles trajectory in detail. The position of the particle can be described by its axial offset r and the angle θ from the axis as shown in Fig. C.2

$$\begin{aligned} r &= r_0 \cos\left(\frac{\omega_L z}{v_z}\right) \\ \theta &= \frac{\omega_L z}{v_z} \end{aligned} \tag{C.6}$$

We can also derive the velocity components from the position as

$$\begin{aligned} v_r &= -r\omega_L \sin\frac{\omega_L}{v_z} z \\ v_\theta &= r\omega_L \end{aligned} \tag{C.7}$$

When escaping the solenoid field, the particle is effected by the same delta distributed radial field as it was when entering, this time with opposite sign. So the effect on velocity is

$$\Delta v_\theta = -r\omega_L \tag{C.8}$$

This means that after going through solenoid, the particle retains only the radial velocity component, though this is only true, if the magnetic field at the cathode surface is zero, otherwise it gains also at least part of the maximum angular velocity. This is undesirable, since it considerably increases emittance, so we design the fields near cathode in a way, that the field is zero at the surface.

What can be also derived from the above equations is the desired length of the solenoid. The solenoid is supposed to be a focusing element, so the radial velocity is negative. This puts constraint on the angular position to be $0 < \theta < \pi/2$, through Eq. C.6 we can derive the length to be

$$l = \frac{\pi}{2}\frac{2m\gamma c\beta}{eB_0} \tag{C.9}$$

From a design point of view, it is much easier to change the field of the solenoid than its length

$$B_0 = \pi\frac{\beta\gamma mc}{le} \tag{C.10}$$

Here we can introduce beam rigidity used to determine properties (strength and bending radius) of dipole bending magnets in circular colliders and could prove to be useful to use here as well since their similarity

$$\begin{aligned} \frac{p}{e} &= \rho B_0 \\ \frac{p}{e} &= \frac{1}{\pi} l B_0 \end{aligned} \tag{C.11}$$

This is still only tentative estimate since the realistic solenoid field doesn't have shape of the step function, but is more smooth at the edges. Also as is mentioned in this appendix, there is some intrinsic emittance and space charge that heavily effect this estimate.

D Space charge

D.1 Transverse forces

For simplicity, let us first consider stable axisymmetric beam with no variation of current density in space or time with current density $j = j_0$ inside the beam and $j = 0$ outside

$$j = \begin{cases} j_0 & \text{if } z \in \mathbb{R} \wedge r \in \langle 0, R \rangle, \\ 0 & \text{otherwise,} \end{cases} \tag{D.1}$$

radius R and particle velocity β. With introduction of the Gauss's law

$$\iiint_V \frac{\rho}{\varepsilon_0} \, dV = \oint_S \mathbf{E} \, d\mathbf{S}, \tag{D.2}$$

we can determine electric forces acting upon particles in the beam. Let us consider a cylindrical surface inside the beam with axis equal to the beam axis height h and radius r. From symmetry of this problem the electrical field is parallel to the bases of the cylinder and is constant and perpendicular to the rest of the surface.

$$\begin{aligned} \frac{\rho}{\varepsilon_0} \pi r^2 h &= E \, 2\pi r h, \\ E &= \frac{r j_0}{2\varepsilon_0 c \beta}. \end{aligned} \tag{D.3}$$

As mentioned above, we discuss not only the electric but also the magnetic field generated by the beam. For that we will use the Ampere's law

$$\iint_S \mu_0 \mathbf{j} \, d\mathbf{S} = \oint_C \mathbf{B} \, d\mathbf{l}. \tag{D.4}$$

Let's consider a circle with radius r perpendicular to and with center equal to the beam axis. Again, from the symmetry of this problem, we can determine that the magnetic field is constant and always tangent to the contour of the circle and from the definition of the problem the current density is also constant and perpendicular to the circle's surface.

$$\begin{aligned} \mu_0 j_0 \pi r^2 &= B \, 2\pi r, \\ B &= \frac{1}{2} r \mu_0 j_0. \end{aligned} \tag{D.5}$$

The electric part of Lorentz force acting upon particles is always repulsive and the magnetic part is always attractive so the radial force is (using relation $\mu_0\varepsilon_0 = c^{-2}$)

$$\begin{aligned} F &= qE - qvB, \\ F &= \frac{1}{2}\mu_0 c j_0 r(\frac{1}{\beta} - \beta), \end{aligned} \tag{D.6}$$

and since $\beta < 1$ the space charge force is always repulsive but with ultra-relativistic beams ($\beta \simeq 1$) can be neglected. This repulsive force is most important to evaluate for beams with high charge density in low energy regions.

D.2 Longitudinal forces

As of yet, we have considered only very simple space and time distribution, so there were no longitudinal forces present, which is not the case for bunched beams which are used in our work. The solution of the above stated Maxwell equations for general beam distribution can't be derived analytically. For that we are using simulation software ASTRA.

The space charge is also one of the limitations of the electron source that we are using, mostly its maximum extracted charge in a bunch, or peak current. For the purposes of this work we mustn't use the Child-Langmuir's law,

$$j = \frac{4\varepsilon_0}{9}\sqrt{\frac{2e}{m_e}}\frac{V^{3/2}}{d^2} \tag{D.7}$$

since the law is only valid under the assumption of zero velocity at the cathode surface, which is not true as was explained in Ch. A, and that there is a DC voltage applied between the electrodes, which is not true since we are using RF gun. Still we can use this law to guide us in our estimations of maximum extracted current. So we have no analytical method to determine the maximum current density for certain RF voltage gradient and frequency.

We can at least determine the longitudinal force acting upon particle on axis at the end of cylindrical beam and from the result can guess the initial parametres for our simulations. Let's consider the same beam as in the previous example but now it has a certain length L.

$$j = \begin{cases} j_0 & \text{if } z \in \langle 0, L\rangle \wedge r \in \langle 0, R\rangle, \\ 0 & \text{otherwise,} \end{cases} \tag{D.8}$$

Here using the Gauss's law won't do as any good, so instead we shall express the z component of electrical field $\mathrm{d}E_z$ of each elementary volume $\mathrm{d}V$ in the base of the cylinder on the axis.

$$\begin{aligned} \mathbf{E} &= \iiint_V \frac{\rho}{|\mathbf{r}|^2}\mathbf{r}^0 \,\mathrm{d}V \\ |E_z| &= \frac{\rho}{2\varepsilon_0}\left(R + L - \sqrt{R^2 + L^2}\right) \end{aligned} \tag{D.9}$$

So in analogy with Child-Langmuir's law

$$j = \frac{2E_0\varepsilon_0\beta c}{R + L - \sqrt{R^2 + L^2}} \tag{D.10}$$

This relation however neglects the fact that the charge distribution in z direction is not constant due to acceleration. What can be considered to be constant is distribution of charge in time, which is coming from the intensity of the laser beam. This is equivalent to known constant current density j so the charge density is

$$\rho(z) = \frac{j}{c\beta(z)} = \frac{j}{c}\frac{1}{\sqrt{1 - \left(\dfrac{mc^2}{mc^2 + eE_0 z}\right)^2}} \tag{D.11}$$

this is the case only if we neglect the effect that the space charge itself has on the distribution, not only in the longitudinal direction but also in the transverse plane too. As stated above, there are no analytical formulas to describe a space charge of general charge distribution and since the distribution evolves in time, this task is done exclusively by space charge tracking simulation codes like above mentioned ASTRA.

Here we show solutions of numerical simulations done in ASTRA for various different settings to show the effect he space charge has on the beam when not compensated.

Since we are using bunched beam not continues beam, we need to define some variables to be able to quantify properties of the beam. The spot size is a size of the bunch in transverse plane and the bunch length is the longitudinal dimension of the bunch. These variables are defined differently for different distributions: for uniform distribution we use the boundaries of the beam, for plateau we often use full-width half maximum (FWHM), for Gaussian and general distribution we use standard deviation (STD). The STD is used for these variables and the Gaussian distribution is used as the initial distribution if not stated otherwise.

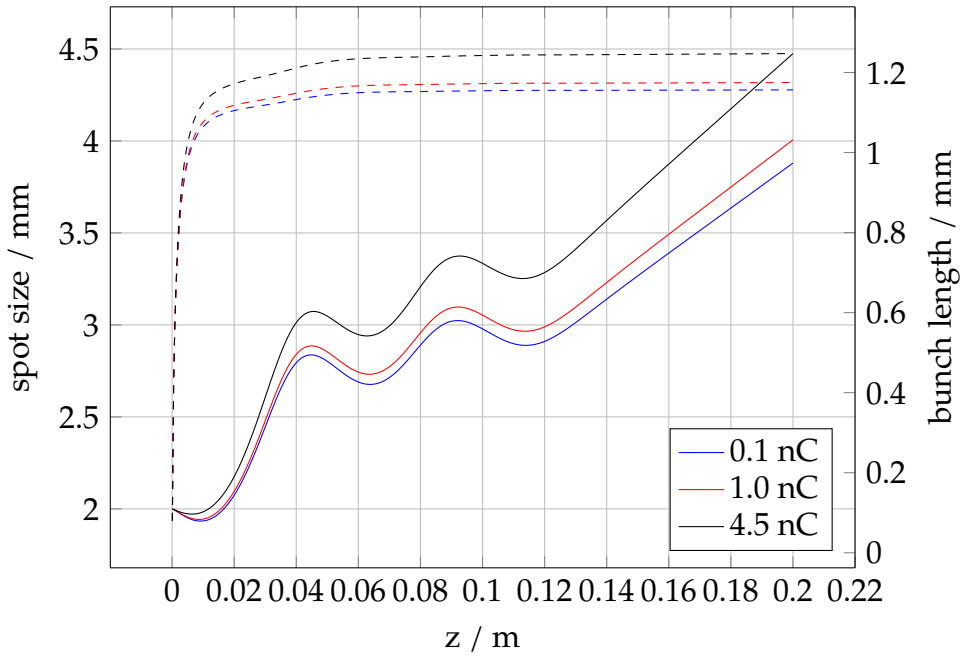

Obrázek D.1: Development of spot size (solid line) and bunch length (dashed line) and its dependence on the bunch charge for initial values of spot size $r = 2\,\mathrm{mm}$ and emission time $t = 15\,\mathrm{ps}$

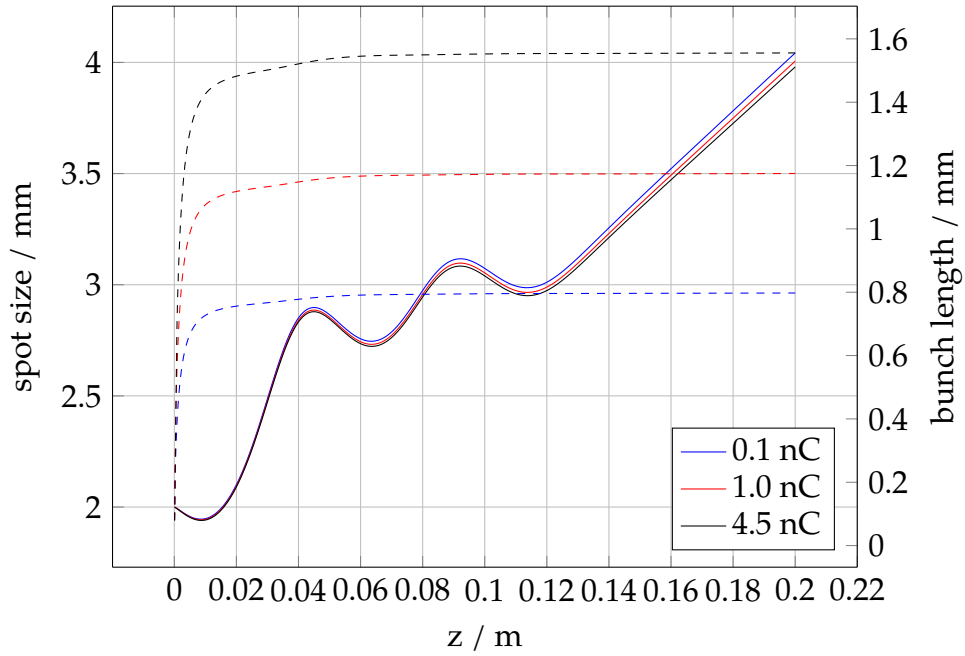

Obrázek D.2: Development of spot size (solid line) and bunch length (dashed line) and its dependence on the emission time [10, 15, 20] ps for initial values of spot size $r = 2\,\text{mm}$ and bunch charge $Q = 1.0\,\text{nC}$

In each these figures, the rising curves represent spot size and the flat top curves represent bunch lengths. The same colour of the curve means it belongs to the same beam simulation with same parametres. In the first one there is a legend to help to guide through the curves. In the other two, legend is missing since the difference is self explanatory. Only one parameter was changed in each figure.

These figures show the development of spot size and bunch length for a beam with different initial parametres. The parametres shared for each simulation are: intrinsic emittance, rise time of the flat-top longitudinal distribution and RF-gun parameters, used for the initial acceleration up to 5,5 MeV, well into relativistic region, with less energy, the program wouldn't be able to track the particles.

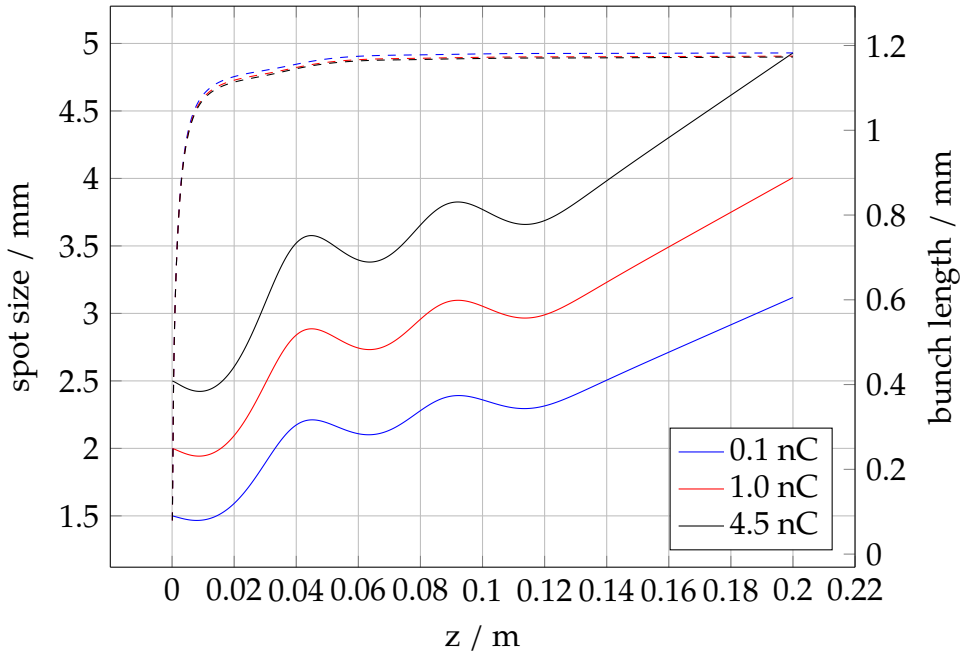

Obrázek D.3: Development of spot size (solid line) and bunch length (dashed line) and its dependence on the initial spot size [1.5, 2.0, 2.5] mm for initial values of bunch charge $Q = 1.0\,\mathrm{nC}$ and emission time $t = 15\,\mathrm{ps}$

In these figures we can clearly see, that there is, for our configuration, a certain value of charge density, for which the space charge forces have significantly more effect. From the first figure there is a factor of 10 and a factor of 5 increase in bunch charge however the difference in effect on the beam is stronger for the lower increase since in absolute terms, the increase its higher. The quick rise of bunch length in the beginning is due to acceleration. If we would take a look at the bunch length in time, we would see steady increase, as is seen in the flat top sections of the figures. Since we are accelerating with RF-gun, the spot size doesn't increase steadily, as would be expected if only the space charge was involved, but there is also some variations. This is due to the focusing effects of RF cavities, which are described in more detail in Sec. 2.3 Ch. 2.

Bibliografie

[1] A. Abada et al. „FCC-ee: The Lepton Collider“. In: *The European Physical Journal Special Topics* 228.2 (červ. 2019), s. 261–623. ISSN: 1951-6401. DOI: 10.1140/epjst/e2019-900045-4. URL: https://doi.org/10.1140/epjst/e2019-900045-4.

[2] A. Einstein. „Über einen die Erzeugung und Verwandlung des Lichtes betreffenden heuristischen Gesichtspunkt“. In: *Annalen der Physik* 322.6 (1905), s. 132–148. DOI: https://doi.org/10.1002/andp.19053220607. eprint: https://onlinelibrary.wiley.com/doi/pdf/10.1002/andp.19053220607. URL: https://onlinelibrary.wiley.com/doi/abs/10.1002/andp.19053220607.

[3] C. N. Berglund a W. E. Spicer. „Photoemission Studies of Copper and Silver: Theory“. In: *Phys. Rev.* 136 (4A lis. 1964), A1030–A1044. DOI: 10.1103/PhysRev.136.A1030. URL: https://link.aps.org/doi/10.1103/PhysRev.136.A1030.

[4] V.V. Paramonov a Aino Skasyrskaya. „Pulsed RF Heating Simulations in Normal-Conducting L-Band Cavities.“ In: *TESLA-FEL Report (2007)*, (květ. 2022).

[5] J. C. Slater. „The Design of Linear Accelerators“. In: *Rev. Mod. Phys.* 20 (3 čvc 1948), s. 473–518. DOI: 10.1103/RevModPhys.20.473. URL: https://link.aps.org/doi/10.1103/RevModPhys.20.473.

[6] Pierre M. Lapostolle a Albert L. Septier. *Linear Accelerators*. Amsterdam: north-Holland Publishing Company - Amsterdam, 1970. xxi, 1197.

[7] Sergey Kutsaev. „Novel Technologies for Compact Electron Linear Accelerators (Review)“. In: *Instruments and Experimental Techniques* 64 (zář. 2021), s. 641–656. DOI: 10.1134/S0020441221050079.

[8] A. P. Banford. *The Transport of Charged Particle Beams*. London: E. F. N. Spon Limited, 1966, s. 9–29. x, 221.

[9] S. Y. Lee. *Accelerator Physics*. 4. vyd. Singapore: World Scientific Publishing Co. Pte. Ltd., 2019. xxxiv, 534. ISBN: 978-981-3274-69-3.

[10] Werner Herr a Bruno Muratori. „Concept of luminosity“. In: (2006).

[11] E. A. Perevedentsev. „Linear beam dynamics and beyond“. In: *AIP Conference Proceedings* 592.1 (2001), s. 6–23. DOI: 10.1063/1.1420408. eprint: https://aip.scitation.org/doi/pdf/10.1063/1.1420408. URL: https://aip.scitation.org/doi/abs/10.1063/1.1420408.

[12] A. Falone, A. Adelmann a L. Stingelin. *RF GUN STUDIES FOR THE SwissFEL INJECTOR*. Tech. zpr. Paul Scherrer Institute, 2011.

[13] Vinit Kumar. „Understanding the focusing of charged particle beams in a solenoid magnetic field“. In: *American Journal of Physics* 77.8 (2009), s. 737–741. DOI: 10.1119/1.3129242. eprint: https://doi.org/10.1119/1.3129242. URL: https://doi.org/10.1119/1.3129242.

[14] Jr. S. Humphries. *Principles of Charged Particle Acceleration*. Albuquerque, New Mexico: John Wiley a Sons., 1999, s. 108–137, 356–500. eprint: http://web.mit.edu/22.09/ClassHandouts/Charged\%20Particle\%20Accel/FRONTMAT.PDF.

[15] Boaz Nash. „Solenoid Fringe Optics“. In: (břez. 2001). DOI: 10.2172/784881.

[16] S. Bettoni, M. Pedrozzi a S. Reiche. „Low emittance injector design for free electron lasers“. In: *Phys. Rev. ST Accel. Beams* 18 (12 pros. 2015), s. 123403. DOI: 10.1103/PhysRevSTAB.18.123403. URL: https://link.aps.org/doi/10.1103/PhysRevSTAB.18.123403.

[17] Jean-Yves Raguin. *The Swiss FEL S-Band Accelerating Structure: RF Design*. Tech. zpr. Paul Scherrer Institute, zář. 2012.

[18] Franz Hagemann et al. „Supercontinuum pulse shaping in the few-cycle regime“. eng. In: (2013). ISSN: 1094-4087. URL: http://dx.doi.org/10.17169/refubium-18770.

[19] T.S. Moss. „Photo-effects in semiconductors“. In: *Journal of Luminescence* 7 (1973), s. 359–389. ISSN: 0022-2313. DOI: https://doi.org/10.1016/0022-2313(73)90075-6. URL: https://www.sciencedirect.com/science/article/pii/0022231373900756.

[20] P. Hartmann et al. „A diffusion model for picosecond electron bunches from negative electron affinity GaAs photocathodes“. In: *Journal of Applied Physics* 86.4 (1999), s. 2245–2249. DOI: 10.1063/1.371037. eprint: https://doi.org/10.1063/1.371037. URL: https://doi.org/10.1063/1.371037.

[21] S. Ramo, J.R. Whinnery a J.A. Whinnery. *Fields and Waves in Modern Radio*. 2. vyd. J. Wiley a Sons, Incorporated, 1953. URL: https://books.google.cz/books?id=1AghAAAAMAAJ.

[22] A. Novokhatski. „Wakefield potentials of corrugated structures“. In: *Physical Review Special Topics - Accelerators and Beams* 18 (říj. 2015). DOI: 10.1103/PhysRevSTAB.18.104402.